Hardware Aspects of Sub-THz Antennas and Reconfigurable Intelligent Surfaces for 6G Communications

Kimmo Rasilainen, *Member, IEEE*, Tung Duy Phan, *Member, IEEE*, Markus Berg, Aarno Pärssinen, *Senior Member, IEEE*, and Ping Jack Soh, *Senior Member, IEEE*

***Abstract*— The need for unrestricted, high-quality, and high-speed communications in planned sixth generation (6G) wireless systems drives the development and research towards the sub-terahertz (sub-THz) bands which so far have been relatively unused for wireless communications applications. Additionally, the sub-THz bands have gained an increasing interest as a potential spectral region at which to go even beyond the well-known Shannon limits. This review paper provides a technological overview on some of the key hardware aspects of sub-THz wireless communications (at 100–300 GHz), namely antennas, reconfigurable intelligent surfaces (RISs), and reconfigurable antenna systems based on state-of-the-art technologies reported in recent literature. Different technologies of antennas and RISs are compared to understand their possibilities and limitations, and to identify the most promising technological approaches to transform 6G from a vision into a commercially viable solution. The paper also presents the authors' interpretations of possible hardware and design trends that can shape the future research directions.**

***Index Terms*— Antennas, beamsteering, leaky-wave antenna, lens antenna, phased array, reflectarray, reconfigurable intelligent surface (RIS), THz gap, transmitarray, wireless links, 6G.**

I. Introduction

SIXTH GENERATION (6G) wireless systems will largely be driven by a focus on the unrestricted availability of high quality and high-speed wireless access. Besides current and pre-5G spectrum bands, the upper millimeter-wave (mmW) (30–100 GHz) and sub-Terahertz (sub-THz) frequencies (100–300 GHz) are bands of interest for 6G [1], [2]. The sub-THz region is foreseen as the ultimate solution to spectrum scarcity and capacity limitations of current wireless systems [3], consequently enabling bandwidth needed to enable envisioned data rates from tens of Gbps to over 1 Tbps. Besides much wider spectral availability, the sub-THz band has also potential to improve network densification and throughput to enable spectrum sharing, and to form the three foreseen cornerstones of 6G: communications, imaging and sensing [4]. While sub-THz coverage is considered for short-range applications due to, e.g., increased free space loss and atmospheric attenuation, communication at the sub-THz band is still possible up to 1 km at 300 GHz under certain assumptions [5]. For longer ranges, 6G systems are expected to be able to switch between transmitting and receiving signals at multiple frequency regions ranging from microwaves to sub-THz [4]. Besides that, it is expected that sub-THz bands from 114 GHz to 300 GHz will become available for use in specific scenarios such as point-to-point backhaul communications, short range communications across displays and rack-to-rack communications in data centers [1].

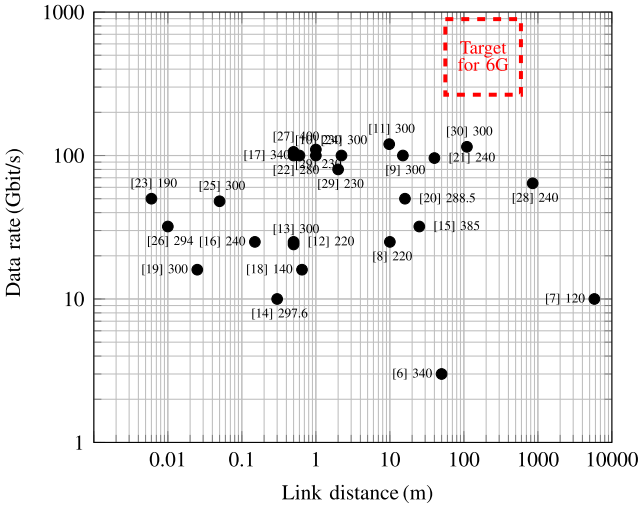

Fig. 1. Link ranges and data rates reported for wireless links above 100 GHz in [6], [7], [8], [9], [10], [11], [12], [13], [14], [15], [16], [17], [18], [19], [20], [21], [22], [23], [24], [25], [26], [27], [28], [29], and [30]. The numbers indicate operating frequencies in GHz.

Fig. 1 illustrates the link distances and data rates obtained by recently reported prototypes at frequencies above 100 GHz in literature [6], [7], [8], [9], [10], [11], [12], [13], [14], [15], [16], [17], [18], [19], [20], [21], [22], [23], [24], [25], [26], [27], [28], [29], [30]. The performance shows quite some spread, and there is no obvious correlation with the used frequency. The compared data rates are peaking around

Manuscript received 1 September 2022; revised 22 March 2023; accepted 16 May 2023. Date of publication 22 June 2023; date of current version 7 August 2023. This work was supported in part by the Academy of Finland through the 6G Flagship Program under Grant 346208, in part by the Academy of Finland through the Academy Project LiBERATE under Grant 346949, and in part by the European Union's Horizon 2020 Research and Innovation Program under Grant 101015956 Hexa-X. *(Kimmo Rasilainen and Tung Duy Phan contributed equally to this work.) (Corresponding author: Kimmo Rasilainen.)*

The authors are with the Centre for Wireless Communications, University of Oulu, 90570 Oulu, Finland (e-mail: kimmo.rasilainen@oulu.fi).

Color versions of one or more figures in this article are available at https://doi.org/10.1109/JSAC.2023.3288250.

Digital Object Identifier 10.1109/JSAC.2023.3288250

or slightly above 100 Gbit/s. Assuming a goal for 6G sub-THz links, e.g., a carrier frequency of 300 GHz, peak data rate up to 1000 Gbit/s and a link distance up to 500 m [31], the red rectangle in Fig. 1 shows that further performance gains are needed even though technology is moving to the correct direction. Facilitating the development of radio communications hardware (HW) to address the Tbps wireless link challenge is essential. Considering the available state-of-the-art HW technologies and their constraints, overcoming this challenge is not straightforward due to the boundaries set by physical and design complexities.

Focusing on the device-to-air interface, key technologies to improve sub-THz wireless links narrow down to three main aspects: 1) Transmitted/reflected gain from antennas and reflectors must be sufficiently high for ensuring a proper signal (re)transmission into air. Conversely, high-gain antennas and reflectors are also needed to detect (possibly weak) sub-THz signals; 2) The antennas and reflectors need to be made reconfigurable (in terms of beamsteering, frequency or both) to support the creation of smart electromagnetic environments; 3) Despite being intended to work in an "intelligent" mode, reconfigurable intelligent surface (RIS) hardware needs to be made reconfigurable and their behavior well-controllable prior to integrating algorithms at a more mature development stage.

Examining the issue of reconfigurability in sub-THz antennas and reflectors more closely, challenges are still abound. Firstly, suitable antenna and reflector topologies need to be carefully selected to ensure sufficient gain levels for sub-THz. Next, several main issues which may result in beamsteering inaccuracies must be considered when introducing this feature onto the selected antenna type. These include beam squinting, frequency drift, thermal effects etc. Due to the changing phases from the beamsteered antennas, closely co-located active components such as amplifiers may also see large changes in impedance, which can affect the performance of the overall RF chain. Therefore, co-designing components in the whole radio front end is now a very important step in ensuring that the required performance can be achieved. Besides that, beam and frequency tuning technologies at sub-THz frequencies are very limited due to a lack of electronics components that have widely been applied at lower frequencies.

This article reviews the key technologies needed to meet the requirements of 6G communications in terms of antennas, beam reconfiguration techniques and reconfigurable reflective surfaces. The benefits, drawbacks, potential, and limitations are presented based on state-of-the-art literature. Aspects related to, e.g., signal processing, algorithms, network planning and measurements are also vital for the deployment of 6G, but these are beyond the scope of the current work. The rest of this paper is organized as follows. Potential antenna implementations for sub-THz applications are presented in Section II. The state-of-the-art and challenges of sub-THz reconfigurable intelligent surfaces are described in Section III. Section IV provides observations made on the hardware, and Section V presents some promising research areas and future trends. Finally, Section VI concludes the work.

II. Directive and Beamsteerable Antennas

In addition to the high path loss, sub-THz links are also known to be highly sensitive to obstacles on the link path. These two properties together with a need to track moving users or to adjust for changes in the propagation environment mean that the antennas need to be beamsteerable. In the following, potential antenna types for sub-THz, beyond-5G applications are introduced, and a comparison between their key parameters is provided. For a general overview of THz antennas, interested readers may consult [32].

A. Lens Antennas

One relatively straightforward approach to meet the high-gain requirements is to use lenses to focus (collimate) the antenna radiation, thereby increasing the directivity [33], [34], [35]. The widespread applicability has faced problems in part due to their sizes. Especially at lower frequencies traditionally used for communications, the needed electrical sizes for lenses can be too large and impractical. At higher millimeter-wave and sub-THz frequencies, these lenses become physically smaller (with comparable performance metrics), which makes their use and integration attractive for more applications.

Two main geometric parameters of a lens which contributes to directivity are: the lens diameter, d_{lens}, which modifies the lens aperture; and its extension height h_{ext}, which varies the location of the feed antenna with respect to the focal point of the lens. While dielectric materials (with $1.2 < \varepsilon_{\mathrm{r}} < 11$) are mostly used for lenses, the focusing properties can also be generated artificially using periodic metal plates or waveguides [37], [38]. Silicon ($\varepsilon_{\mathrm{r}} = 11.9$) lenses are most commonly adapted, especially in sub-THz applications. However, increasing the permittivity also increases the contrast in refractive index at the lens-to-air interface, which causes additional reflections [39]. As a solution, an anti-reflective coating, which are normally $\lambda/4$ thick can be used, at the expense of narrower bandwidth [40]. Besides permittivity, the loss tangent ($\tan\delta > 0.001$) can significantly limit the performance especially if very large (i.e., high-gain) lenses are to be used.

For certain applications, lenses made from inhomogeneous materials provide useful functionalities. Such materials/applications include multi-shell lenses, gradient-index (GRIN) lenses, or lenses with a more specifically defined refractive index profile such as the Luneburg lens and the Maxwell fish-eye lens. Fig. 2 visualizes the principal functionality of conventional homogeneous lenses and inhomogeneous Luneburg and Maxwell fish-eye lenses. In all cases, it is assumed that there are N antennas to generate (up to) N beams. With the conventional lens, the achievable steering range is limited both by the feeding array and the focal properties of the lens. The Luneburg lens collimates rays that emanate from a point source on the surface and, conversely, focuses plane-fields to a point on the surface. A hemispherical Maxwell fish-eye lens collimates rays from a point on its surface, and a fully spherical lens focuses the rays from a point on the surface to the opposite point on the same surface. The properties of the Luneburg and Maxwell lenses, which

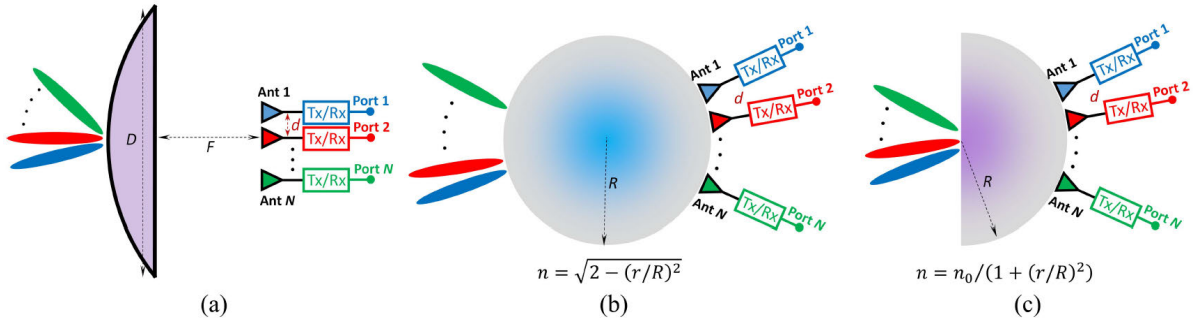

Fig. 2. Conceptual illustration of (a) regular homogeneous lens, (b) Luneburg lens with gradient-index material, and (c) Maxwell fish-eye lens with gradient-index material. An array with N elements is used to generate N different beams. Reprinted from [36] ©2017 IEEE.

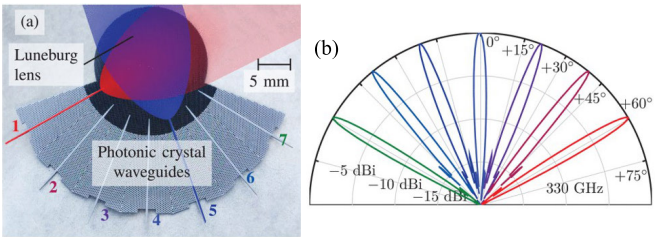

Fig. 3. A seven-port Luneburg lens antenna: (a) photo of fabricated antenna showing beams launched from ports 1 and 5, and (b) measured 330-GHz radiation patterns. Reprinted from [41] ©2019 IEEE.

are examples of multibeam antennas [36], allow simultaneous generation of multiple beams to different directions.

The work in [41] presents an integrated Luneburg and Maxwell fish-eye lenses operating at 330 GHz. The antenna consists of a Luneburg lens-based multi-beam antenna and a Maxwell fish-eye lens-based slab-mode beam launcher as shown in Fig. 3, and can provide a total beamsteering angle up to 120° (60° each side) at intervals of 20°. A compressed Luneburg lens operating at 75–110 GHz range was reported in [42]. The antenna is fabricated through multimaterial 3D printing technology using five different dielectric filaments. With an open-ended waveguide probe excitation across the 75–110-GHz band, the antenna shows a boresight gain of 22 dBi, and a –3-dB scan angle of 25° at 84 GHz.

In multi-shell lenses, shells made from different materials are assembled together to form a suitable refractive index profile. Gradient-index (GRIN) lenses are typically cylindrical in shape, and the radial refractive index profile can be obtained, e.g., by 3D printing concentric cylinders of varying permittivity [43] or by etching a pattern of holes in Si wafers [44], [45]. 3D printing is more suitable for lower mmW frequencies (e.g., Ka band), whereas the wafer patterning approach has been implemented above 200 GHz as well. Fabrication accuracy and properties of the used processes are key practical challenges when implementing inhomogeneous lenses, and when two or more different materials are involved, properties such as compatible thermal and mechanical expansion coefficients can be important in some applications. Especially at lower frequencies where the lenses are physically large, estimating the weight of the different shells is an important factor [46].

Recently, geodesic lenses have been studied to mimic the operation of 2D rotationally symmetric GRIN lenses using a 3D structure to produce an operation similar to Luneburg lenses. Unlike the Luneburg lens, it is possible to fabricate geodesic lenses from metal, which can be advantageous to achieve radiation efficiency higher than with dielectric lenses as the frequency increases [47], [48]. Metalens antennas are another solution to overcome the bulky design of classical dielectric lens antennas. A metalens is a flat surface that can control EM waves using the phase compensation method. Compared to conventional bulky dielectric lenses, metalens antennas offer much more flexibility with their planar design and fabrication as they can produce spherical phase in the plane and replace the complex feeding structure with a waveguide or a new coupler structure. For example, the work of [49] presented a dual-band Fresnel zone plate metalens antenna fabricated based on low-cost additive manufacturing. The measured peak gain at 120 GHz is 21.9 dBi.

For high gain and beamsteerable lenses, three main design strategies can be identified: fixed-beam lenses, switched beam lenses, and steerable beam lenses. The most conventional fixed-beam lens can be designed by integrating and optimizing a lens and feed antenna to meet the performance requirements for, e.g., directivity and beamwidth. In the second category, a switched-beam lens uses a group of feeding antennas that are connected through a switch network to select the desired feed and resulting beam direction. Here, a proper design for the feed network is essential since the losses introduced by the transmission lines and switches can start to degrade the directive gain provided by the lens itself. The third type utilizes beamsteering to control the direction of the radiated beams. While this concept shares some of its features with switched-beam designs, the main difference is that the array of feed antennas can allow for a more continuous steering instead of discrete directions of switchable fixed beams.

In [50], a 2D feed array is used at 450 GHz for phase shifting and antenna displacement. This approach makes the beam highly directive and gives a fine scanning resolution in two planes, as well as a low power consumption. A peak directivity of 26 dBi with angular scanning capability of ±28° and ±8° in E and H-plane, is produced, respectively. The scanning range can be modified by scaling the array size. With multi-element feed arrays, not all elements are in the lens focus simultaneously, and the physical offset of the outer elements can start to limit the performance. As discussed in [51], a key

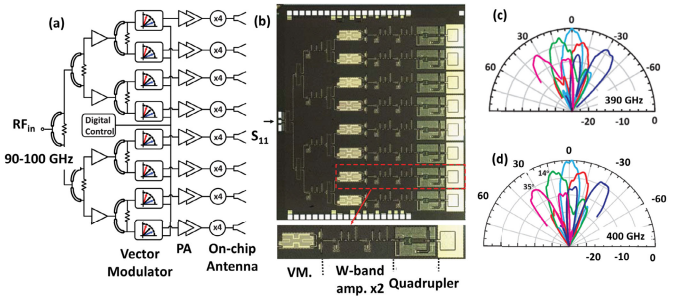

Fig. 4. Sub-THz phased array antenna: (a) block diagram, (b) microphotograph with a zoom-in on a single channel, and H-plane radiation patterns at (c) 390 and (d) 400 GHz. Reprinted from [56] ©2016 IEEE.

effect is the physical offset relative to the lens size. This explains why the lens and array gain does not always increase with the number of array elements (unlike in conventional arrays without lens). The element displacement reduces the gain and starts to steer the beam away from boresight. However, this effect can be compensated for by using a larger lens, as it provides smaller relative displacements [52].

B. Phased Arrays

A phased array antenna consists of multiple antenna elements which are coherently fed using phase shifters at each element. This enables them to electrically scan their beam to desired directions [53]. Besides serving as a planar alternative to conventional lenses for improving the directive gain, phased array antennas also offer better electrical beam-steering capability, which is very useful for narrow beam antennas to expand their coverage. The fundamental operating principle of the phased array is the superposition of the radiated phases from different antenna elements. A combination of in-phase elements forms a radiation of additive amplitude, whereas elements radiating out-of-phase cancel each other out [54].

Phased array antennas are a good solution in the microwave regime to implement beamsteering and high gain. However, when operating at the higher sub-THz band, the high losses of the semiconductor switches starts to constrain the phase-shift application [55]. Several solutions have been proposed to overcome this, such as shifting the phase before upconverting the frequency to THz frequencies [56], developing spatial phase modulators based on tunable materials such as graphene [57] or taking advantage of optical technology to design optical true-time delay (OTTD) phase shifters [58].

The first method of phase shifting in a phased array to enable electronics-based beamsteering is demonstrated at 400 GHz using CMOS technology, as shown in Fig. 4 [56]. The beamformer consists of a W-band distribution network with vector modulators that are used as phase shifters, and amplifiers are connected with the antenna elements via a linear eight-element quadrupler array as shown in Figs. 4(a)–(b). The antenna achieved an equivalent isotropic radiated power (EIRP) of more than 5 dBm at 375–405 GHz with a peak EIRP of 7–8.5 dBm at 380–400 GHz. Moreover, it offers beam steering angle of 70° in one plane (35° on each side). Next, the work of [57] proposed a low-profile graphene-based beam-steerable phased array antenna at 150 GHz. The array is composed of a pair of dipole antennas coupled symmetrically to the feed point through a co-planar strip-line (CPS) and two graphene sheets loaded at the lower boundary of the CPS. The chemical potential of the graphene sheets is tuned individually using two adequate DC biasing voltages to steer the beam to desired angle(s). The simulation shows that when varying the chemical potential from 0 to 0.2 eV, beamsteering of 44° (22° each side) was achieved at 150 GHz in the E-plane.

Finally, beamsteering using a true-time delay (TTD) optical beamforming network (OBFN) for a phased array antenna at 300 GHz was presented in [58]. The input at the optical band is directed to TTD to produce a modulation bandwidth prior to being channeled to the phase shifters. These optical signals are then converted to RF signals at the 300-GHz band by Indium phosphide (InP) photomixers and consequently radiated by the 1×4 array antenna. Thus, the phase shift of the optical signals allows changing the phases of the generated RF signals for beamsteering via the antenna array. Simulations indicated that steering angles up to 70° are possible. The work in [59] developed an optical phased array (OPA) chip based on the thermo-optic effect of a silica waveguide. The silica waveguides work as optical phase shifters (OPS) via its refractive index changes when heated. Consequently, the change of the optical input phase is proportional to the power consumption of the heater after the OPS. By using such an OPS, the feasibility of continuous 300-GHz beamsteering is successfully demonstrated across a range of 50°. Moreover, a hybrid electromechanical scanning lens array was proposed in [60] at 550 GHz with a total scanning angle up to 50° (25° each side). The concept relies on combining electronic phase shifting of a sparse array as a feed to simplify the RF front-end with a mechanical translation of a lens array.

When upscaling a phased array from mmW (e.g., 28 GHz) to the sub-THz band (up to 300 GHz), a reasonable array with 32 elements at lower frequencies is expected to require an array with thousands of antenna elements in the latter case. The elements also require a comparable number of parallel transmit and receive RF paths [5]: this complexity together with the power consumption will strongly limit the practical implementations at and scalability to the sub-THz band.

C. Reflectarrays

Reflectarray antennas share the spatial illumination characteristics of reflector antennas and the phase synthesis and beam collimation features of antenna arrays, making them hybrid structures that incorporate the advantages of both reflectors and printed arrays while overcoming their respective limitations [61], [62], [63]. The antenna elements are designed to reflect the incident field with certain phase shifts so that when the feed spatially illuminates the aperture, it will collimate the beam to the desired direction with the desired beam shape.

Besides their advantages over reflectors and fixed-beam arrays (discussed in detail in [61]), reflectarrays can also be used effectively in beam scanning applications. The stringent requirements imposed by conventional high gain beam scanning architectures on the antenna radiation capabilities makes very few antenna types suitable for such applications.

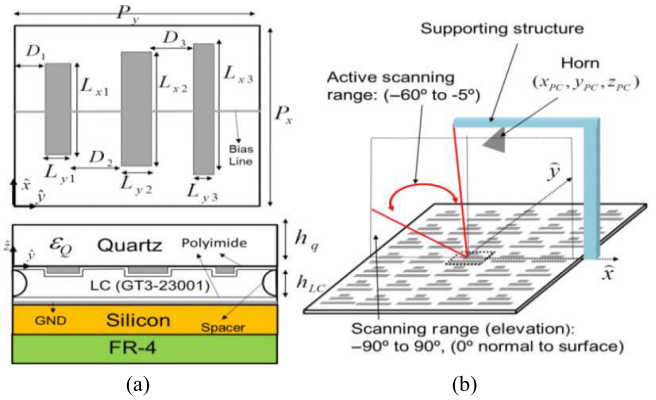

Fig. 5. Schematic of a liquid crystal (LC) reflectarray antenna: (a) top and side views of the unit cell, (b) proposed reflectarray antenna configuration. Reprinted from [65] ©2015 IEEE.

Normally, depending on the required scan rate, scan volume, and cost, lenses, reflectors including parabolic and reflectarray antennas and phased arrays are the choices for most high gain and beam scanning applications. Based on these principles, different variants of reflectarrays have been introduced.

The first example is a folded reflectarray proposed in [64] which is made reconfigurable using liquid crystal (LC) technology. The antenna consists of a lower reflector incorporated with a feed centered on its planar structure. A polarizing grid is then integrated on the top as its upper reflector. The lower reflector collimates the beam and twists the polarization. The top grid then selects the polarization for the transmission and reflects the orthogonally-polarized waves towards the lower reflector. This combination enables additional phase adjustment for beamsteering on the upper reflector. The upper reflector is integrated with an LC mixture that can be tuned via voltage biasing to obtain an appropriate phase adjustment and result in beam steering. The main beam can be steered towards $\pm 6^\circ$ at 78 GHz with 25.1 dB of measured gain.

Several other beam-steerable reflectarray antennas using LC have been proposed at 100 GHz [65], [66]. The work in [65] proposed a LC-based reflectarray antenna composed of 54×52 multiresonant unit cells. As seen in Fig. 5, the proposed reflect array unit cell has three parallel unequal length dipoles printed on the lower surface of a quartz wafer. A cavity is formed between the quartz and silicon wafers, and a tunable layer is formed by filling this cavity with LC material. Furthermore, the upper surface of the silicon wafer is metallized to form a ground plane. The permittivity of the LC layer is voltage-controlled, which therefore controls the phase of reflection coefficient in the unit cells. The antenna can provide a wide 55° angular beam scanning at one plane, as well as a large bandwidth with reduced side lobe levels from 96 to 104 GHz.

Another folded reflectarray structure has been implemented at 390 GHz in [67]. In this design, a horn antenna is used to feed the THz signal, which is then reflected back to the aperture of the reflectarray using a grid polarizer. Next, a reflective metasurface rotates the polarization by 90° to produce a pencil beam to go through the polarizer. Beamsteering or custom beam patterns can be achieved by suitably designing the reflective metasurface, though only a boresight pattern is reported in the work. Using this concept, the overall antenna profile can be made smaller, and the different parts can be separately fabricated to simplify the process and potentially lower the cost. Another folded reflectarray operating at 1 THz was proposed in [68], utilizing a unit cell based on an anisotropic dielectric resonator antenna to produce a planar wavefront and to achieve the 90° polarization twist to pass the signal through the grid polarizer.

The phase shift required in a reflectarray can be obtained using specifically designed antenna elements or switches. In [69], a 120-GHz reflectarray is proposed, where the phase shifts are implemented using open- or short-circuited conductor-backed coplanar waveguide stubs. The reflectarray elements can be switched between four phases: 0°, -90°, -180°, and -270°. Another reflectarray studied the use MEMS elements for beamsteering applications at 300 GHz [70] where the genetic algorithm was also deployed to maximize the directivity and minimize the sidelobe level. As a result, simulations achieved a directivity of 16.7 dBi while the sidelobe level was significantly suppressed from –13.7 dB to –16 dB. Next, the work of [71] discusses techniques to improve the performance of sub-mmW reflectarray by eliminating unwanted resonances. In the reflectarray, the generation of surface waves and higher-order modes can distort the element pattern, which causes phase error in the reflected signal. The proposed solution to overcome these issues and improve the gain and bandwidth performance is to implement sub-wavelength unit cells, which was experimentally demonstrated at W-band.

Reflectarrays consisting of dielectric elements have also been proposed due to their ease of fabrication using 3D printing technology. One such example is the reflectarray antenna designed at 220 GHz in [72], which consists of dielectric unit cell blocks backed by a metal sheet as the ground plane. It achieves a gain and bandwidth of 31.3 dBi and 20.9%, respectively. In addition to dielectrics, graphene is another material used to build reflectarrays and to simultaneously integrate the reconfigurability feature in them [73]. However, this method and reflectarray has been demonstrated for operation at a relatively high frequency of 0.8 to 1.2 THz. The complex conductivity of graphene is controlled by adjusting the electric field. This then enables changing the phase and the resonance point of the reflected or transmitted wave on the element, which results in beam reconfiguration.

D. Transmitarrays

The transmitarray antenna combines the favorable features of array and lens antenna techniques to result in a low-profile conformal design with versatile radiation behavior while maintaining a high radiation efficiency. In general, it combines a thin, flat transmitting surface illuminated by a feed source located on an equivalent focal point. The transmitting surface is integrated with an array of antenna elements, where the unit cells are individually designed to convert the spherical phase front originating from the feed to a planar phase front. This then results in a focused radiation beam with high gain and steerable transmitted beam.

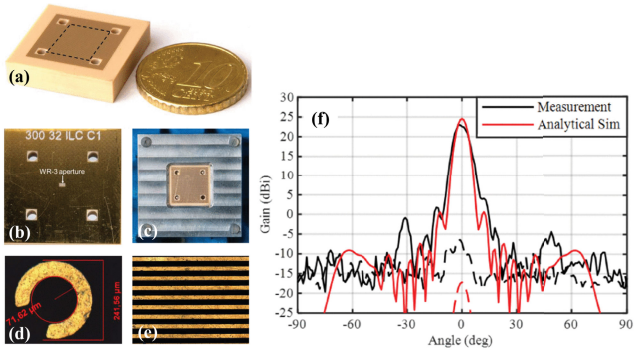

Fig. 6. H-band (225–325 GHz) substrate-integrated transmitarray antenna: (a) Full view of prototype with the unit cells area outlined. (b) Bottom metal layer showing the waveguide aperture. (c) Front view of the prototype mounted on the test frame. (d) Cell 045 resonator. (e) Top grid. (f) Radiation pattern in E-plane. Reprinted from [75] ©2021 IEEE.

Similar to reflectarrays, the unit element design determines both the resulting magnitude and phase coming out of the transmitarray. The phase of each array element can be controlled individually by varying its dimensions, but phase compensation cannot be achieved by only a single transmissive layer [74]. Therefore, the three most common design methods to effectively control the phase of the waves in transmitarrays are multi-layered frequency selective surfaces (M-FSS), receiver-transmitter (Tx-Rx) design, and metamaterial/transformation approach, also known as metalenses [74].

In reflectarrays, a metallic ground plane reflects most of the incident waves, which produces a reflection magnitude typically close to unity (0 dB) [74]. Therefore, the main parameter to control is only the reflection phase from each element. In contrast, both (transmitted) magnitude and phase need to be controlled well (with magnitude close to unity) to maintain a high efficiency in transmitarrays. Depending on the application, both transmit- and reflectarrays can be integrated into various platforms in the environment and objects, such as walls, windshields of vehicles, aircrafts, unmanned aerial vehicles (UAVs), and public transportation systems as they can be designed using conformal materials.

An example of the multi-layered transmitarray antenna in sub-THz is [75] operating at H-band (225–325 GHz), as illustrated in Fig. 6. The antenna is designed on a single printed circuit board (PCB) stack with five metal layers and multiple low-loss dielectric substrates in a monolithic module. The highest achieved gain and 3-dB gain bandwidth are reported to be 23.1 dBi and 17.2% at 332 GHz, respectively. Besides that, the antenna exhibits linearly-polarized pencil-beam radiation patterns with low side lobes and low cross-polarization characteristics. Several other multi-layered transmitarray antennas reported in [76] and [77] comprise of three metal layers and two interleaved dielectric spacers. The prototypes are fabricated using a standard PCB process. Measurement results demonstrated that this design methodology is effective even under strict technological constraints. The antenna achieved a peak gain above 32 dBi with an aperture efficiency above 36%.

The Tx-Rx design approach, on the other hand, is demonstrated in [78], presenting a D-band transmitarray antenna with Tx-Rx unit cells designed using low-temperature co-fired ceramic (LTCC) technology. The unit cell includes a pair of wideband magnetoelectric dipoles as the receive/transmit elements connected by phase shifters, providing a full-range phase change from 0° to 360°. The measured peak gain of the proposed antenna is 33.45 dBi at 150 GHz with an aperture efficiency above 44% and a 3-dB gain bandwidth of 24.29%.

The last category of transmitarrays, the previously discussed metalens, has also been reported. An example is the work of [79] that proposes a method to synthesize, design and characterize a metalens-type transmitarray antenna at 300 GHz. By designing suitable feed and focal distances, a broadside pencil beam with reduced sidelobe levels is achieved. To the best of the authors' knowledge, this is the first experimental validation of the proposed approach, with a design of 400 elements on the transmitarray that combines eight different types of unit cells (resulting in a 3-bit phase quantization). Measurement results are in good agreements with simulations, indicating a 25.5-dBi gain with an aperture efficiency of 28.2%. Another metalens-type transmitarray reported in [80] is designed and fabricated using low-cost PCB technology. The transmit array uses a two-layer element that can provide full-range phase coverage of 360° and a transmission coefficient better than –3.52 dB at 250 GHz. The proposed antenna produces a peak gain of 28.8 dBi and aperture efficiency of 32%.

It is worth noting that because of technological constraints and simplicity of fabrication, most available works on transmitarrays are manufactured using a standard PCB process. Due to tighter dimensional tolerances for designing such antennas at the sub-THz band, this factor needs to be carefully considered to avoid degrading the final antenna performance. An example of this is the reported phase shift error of 15° due to fabrication tolerances of PCB technology (±10 μm) at H-band [75].

E. Leaky-Wave Antennas

Leaky-wave antennas (LWAs) are a subset of a more general group of traveling-wave antennas, and they have differences in terms of the wave behavior and radiation mechanism; examples of traveling-wave antennas include waveguide slot antennas, helical antennas, and dielectric rods [37]. Compared to the previously discussed antenna types, LWAs do not require complex feed control circuits, such as phase shifters or true-time delay feeding networks. This is due to the fact that the beams are steered depending on the carrier frequency. As a result, LWAs are simpler to design and less costly, features which have major commercial advantages. LWAs are expected to be an appealing solution at THz frequencies for applications such as THz interconnects, which require robust and highly integrated THz beam steering antennas [81]. For an overview of LWAs, interested readers may consult [82]. In general, the non-resonant nature of the radiation mechanism and guided waves (GW) are two aspects which work together to provide a wide operational bandwidth. For example, one-dimensional (1D) linear arrays of LWAs are capable of producing scannable pencil beams in the elevation and azimuth planes [83]. On the other hand, two-dimensional (2D) LWAs can produce either broadside pencil beams or conical scanned beams [84].

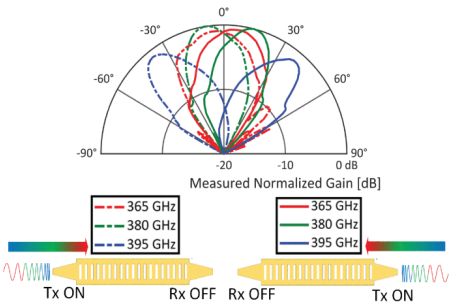

Fig. 7. Measurement results of a dual-port chip-integrated waveguide (CIW)-based leaky-wave antenna for one-shot simultaneous localization of multiple wireless nodes operating at 360–400 GHz. Reprinted under CC BY 4.0 license from [86] ©2021 Authors.

To date, only few THz LWAs have been reported, and these are designed on either polymer or graphene substrates. For example, the work of [81] presents an LWA made up of periodic leaking microstrip lines and a grounded coplanar waveguide to microstrip line transition. Intended for future integration with InP-based photodiodes, its operating frequency was changed from 230 to 330 GHz to enable a quasi-linear beam tuning from –46° to 42°, (with a total scanning angle of 88°). Measurements of the fabricated prototype indicated an average realized gain of –11 dBi and a 3-dB beamwidth of 10° (using a 1.5-mm wide InP LWA). On the other hand, a graphene-based LWA was designed to operate at a fixed frequency in [85]. DC biasing on the pads of the structure was implemented on the leaky mode by sinusoidally modulating the graphene surface reactance. This change in voltage allows modifying the leakage rate and consequently the main beam direction. However, it should be noted that this conceptual work involves only theoretical calculations and simulations, without results on an experimental implementation.

Recently, a dual-port LWA operating at 360–400 GHz has been reported for localizing applications [86]. As shown in Fig. 7, the antenna has two dual-port LWAs. Therefore, the transmitter and receivers can be integrated on the opposite ends of the LWA (e.g., Ports 1 and 4 are transmitting while Ports 2 and 3 are receiving). This allows one-shot simultaneous localization of multiple wireless nodes. The transceiver and antenna are fabricated in a 65-nm bulk CMOS process. The measured one-shot localization error variances in 1D and 2D spaces are less than 1° with 200-Hz resolution bandwidth and less than 2° with a 20-Hz resolution bandwidth, respectively.

III. Reconfigurable Intelligent Surfaces (RISs)

Reconfigurable intelligent surfaces (RIS) have mainly been referred to as two-dimensional (2D) structures that can dynamically manipulate the impinging electromagnetic (EM) waves. To achieve this, RISs are integrated with phase/amplitude tunable unit cells to control the incident waves through various mechanisms such as voltages, thermal, optical or mechanical. The arrangements of the unit cells can be modified and programmed in response to external stimuli.

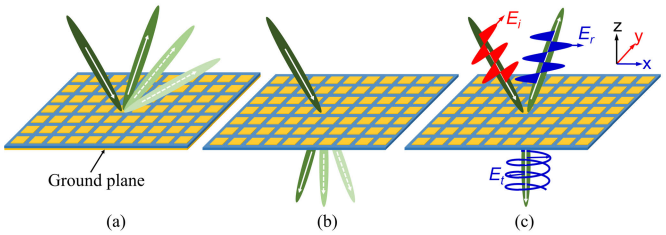

Fig. 8. Schematic drawings of (a) reflecting RIS, (b) transmitting RIS, and (c) RIS working as a polarization converter.

A. Operating Modes and General Properties of RIS

The definition of RIS and its working principle has been extensively discussed in [87], [88], [89], [90], [91], [92], [93], [94], and [95]. However, most of these RISs operate as a reconfigurable reflecting surface. Nevertheless, reconfigurable reflecting, transmitting, and polarization conversion surfaces, as illustrated in Fig. 8, can be considered as a RIS if external stimuli (e.g., artificial intelligence) can be integrated into their control mechanisms to control the EM propagation for improved overall system performance. Among these features of RIS, reflecting and transmitting RIS are envisioned to have a broader applications and will be discussed more detailed in this paper. The principle and analysis of polarization converters can be found in, e.g., [96], [97], and [98].

Two principal hardware design paths for RIS found in literature based on either traditional antenna arrays or metasurfaces. The unit cell of antenna array-based RIS has a resonant size close to $\lambda/2$, meanwhile metasurface-based RISs consist of a large number of closely spaced sub-wavelength (e.g., $\lambda/10$ [99]). The operation of the metasurface-based RIS is based on diffraction to split the incident EM wave into a few components whose number and directions depend on the angle of incidence, wavelength and the period of the unit cells. Recently, the metagrating concept has been proposed in [100], using a periodic array of carefully designed scatterers. Compared to conventional metasurfaces, the distance between unit cells of metagratings is comparable with wavelength and does not need a continuous gradient surface impedance. This makes metagratings much simpler to fabricate, and shows their strong potential for sub-THz operation even though the technology is still less mature than the two previous approaches.

B. Overview of Key RIS Parameters

For the hardware, one of the most significant parameters to evaluate a RIS is the *efficiency* (η), defined as the ratio between the power reflected/transmitted to a desired direction and the total incident power. Other key parameters of a RIS are its *steering range* and *angular resolution*. The steering range depends greatly on the technique: e.g., mechanical steering with (partially) movable components may provide a wide steering range up to 360°, whereas an electronic approach typically has a more limited steering range at its operating band, e.g., around 120° [101].

Meanwhile, the angular resolution mainly depends on the main lobe beamwidth, which depends on the number of phase quantization bits and the number of unit cells. The quantization

is affected by the number of integrated switches. The number of unit cells has an impact on the aperture size and periodicity of the RIS: with the same aperture, switching the periodicity from sub-wavelength ($\lambda/8$, similar to metasurfaces) to $\lambda/2$ (similar to reflectarrays) greatly reduces directivity [66].

Finally, the *power consumption* of a RIS is also an important consideration. This includes power to the controller and power consumed for each actuator on a unit cell (e.g., transistors, diodes, pumps, and motors). For active RISs, significant amount of power may also be needed to amplify the incident signal prior to reconfiguration and reflection/transmission.

C. Possibilities of RIS for Sub-THz Communications

Increasing carrier frequencies make wireless propagation more challenging due to the higher propagation and penetration losses and lower levels of scattering. This leads to fewer useful propagation paths between the transmitter and receiver. In such situations, RIS can be deployed to improve the propagating conditions by introducing additional passive beamforming towards the desired receivers, improving gain and suppressing co-channel interference [102], [103]. Such a RIS can ideally be designed in a smart, programmable, and controllable way for creating new degrees of freedom to complement existing high-gain transmit/receive antennas and create a truly smart wireless propagation environment.

Similar to the existing relay technologies, RISs can relay and redirect EM waves without causing any noticeable propagation delays, except for some increase in the channel delay spread [104]. The work of [104] compares in detail the capacity between conventional single-input single-output (SISO), relay-supported, and RIS-supported transmissions. The conclusion from [104] is that ideally, the transmitter or receiver should be within the line of sight (LOS) of the utilized RIS. Provided that the number of elements is large enough, the RIS-supported scenario shows a significantly lower transmit power required to achieve the same rate compared to conventional SISO and relay-supported channels. Since the surface needs to be physically large relative to a classical half-duplex relay, RIS can potentially improve the propagation conditions in short-range communications, particularly at sub-THz and THz bands. For example, RIS can strengthen the propagation even when the LOS path is blocked. However, its use case in non-LOS scenarios is equally important, e.g., to increase the rank of the channel to achieve full multiplexing gain [105].

Fig. 9 shows potential RIS applications including transmitting in an indoor scenario and reflecting in an outdoor case. These RISs can be installed on windows/walls to split/steer incident EM waves from a base station (BS) towards users. By jointly optimizing the environment through the use of RIS together with transmitters and receivers, the wireless system performance may surpass the limits postulated by the conventional Shannon theory. This approach has the potential to enhance the efficacy and capacity of wireless communication systems beyond the bounds of current theoretical predictions.

D. State-of-the-Art Sub-THz RIS Implementations

To make the surface reconfigurable, each unit cell or group of unit cells (referred to as a "super cell") needs to be

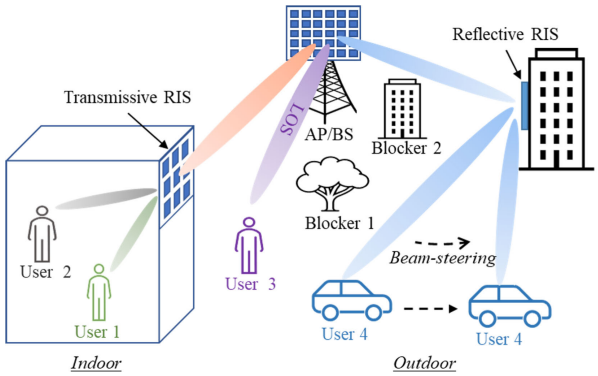

Fig. 9. Illustration of RIS-supported transmission for 6G communications. In an indoor scenario, a transmissive surface splits the incident BS signal to different transmitted beams towards different users, and in an outdoor scenario, a RIS can steer the reflected beam to a moving user.

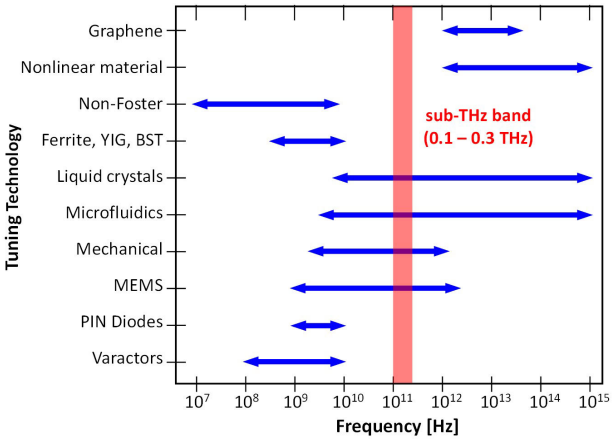

Fig. 10. Tuning technologies for RIS versus working frequency. The targeted sub-THz band is shown in red. Adapted from [106] ©2015 IEEE.

individually tunable to a certain state to manipulate the waves incident to the RIS. Suitable tuning technologies for the unit cells or super cells depend heavily on the operating frequency, as illustrated in Fig. 10. In light of this information, the most suitable tuning technologies for RIS working at the sub-THz band are micro-electromechanical system (MEMS), mechanical approach, liquid crystal, and microfluidic approaches. It is worth to note that the active elements (e.g., PIN diodes) commonly used in the microwave regime are impractical at the sub-THz band due to their limited cutoff frequencies and higher losses [107]. Alternatively, complementary metal-oxide-semiconductor (CMOS) transistors, Schottky diodes, or high electron mobility transistors (HEMTs) can also be implemented on RISs for operation at this band.

Recent demonstrations of the RIS at sub-THz band can be found in, e.g., [101] and [107]. The work in [107] demonstrates a large-scale programmable metasurface using arrays of CMOS-based chip tiles at 300 GHz. Each unit cell is a split-ring resonator which consists of 8 transistors working as switches that enable programming the unit cell to realize 84 different structures, thereby changing the amplitude and phase response. Moreover, eight sub-wavelength inductive loops are added to each unit cell, enabling the switches to operate beyond their cutoff frequency, reaching up to 5 GHz.

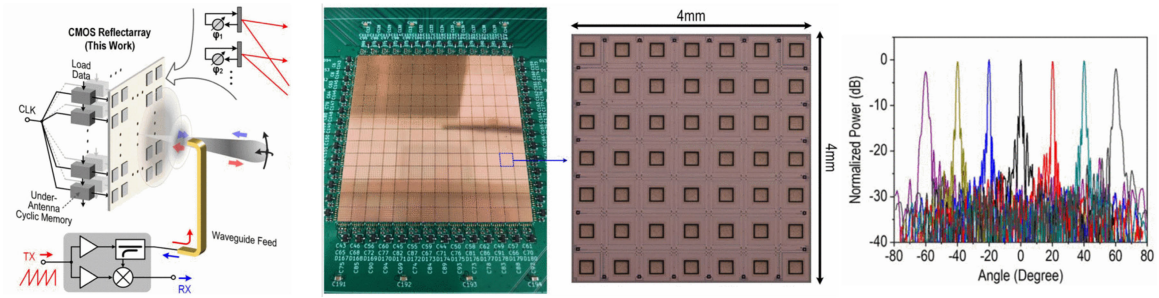

Fig. 11. Reflectarray-based reflective RIS working at 265 GHz: (a) Schematic, (b) Fabricated prototype, and (c) Measured radiation patterns of electronically-scanned pencil-beam steering in E-plane. Reprinted from [101] ©2022 IEEE.

TABLE I
COMPARISON OF DIFFERENT RIS SOLUTIONS AND TECHNOLOGIES DEMONSTRATED EXPERIMENTALLY AT SUB-THZ FREQUENCIES

Ref.	RIS type	Design approach	Freq. (GHz)	Periodicity (λ)	Aperture size (λ^2)	Reconf. technology	Beam-steering angle ($^\circ$)	Efficiency (%)	Fabrication technology
[107]	Transmissive Passive*	Coding metasurface	300	0.14	3.36×3.36	Transistors	30	30	65-nm CMOS
[101]	Reflective Passive*	Phased array	265	0.5	49×49	Transistors	60	N/A	22-nm CMOS
[108]	Transmissive Passive*	Metasurface	300	0.08	0.4×0.4	Transistors	N/A	N/A	180-nm CMOS
[109]	Reflective Passive*	PAR**	140	1.15	32.6×32.6	N/A	60	89	PCB
[110]	Reflective Passive*	Coding Metasurface	300	0.23	5.75×5.75	Vanadium dioxide	30	N/A	Photolithography
[111]	Transmissive Passive*	Coding Metasurface	408	0.82	21.12×21.12	Liquid crystal	30	40	Photolithography
[96]	Polarization Passive*	Coding Metasurface	190	0.63	19×19	Microfluidic	14	N/A	Photolithography

*Without power amplifiers. **Perfect Anomalous Reflector (PAR) achieved via impedance matching optimization.

A single chip tile features 12 × 12 unit cells. The final metasurface structure consist of a 2×2 array of tiled chips with a total of 576 unit cells fabricated in a 65-nm industry-standard CMOS process. The unit cells are individually addressable and are digitally programmable with 8 bits of control at GHz speed. Additionally, both the amplitude and phase response of each unit cell can be independently controlled, allowing a beamsteering angle of 30° on each side. Another recent work reported a pencil beam 2D beamsteering reflectarray at 265 GHz [101] as illustrated in Fig. 11. The reflectarray consist of 98×98 half-wavelength-spaced elements fabricated on CMOS chips. The experimental beamwidth and steering angle of the reflectarray are 1° and 60°, respectively, to each side.

In general, only few sub-THz RISs have been demonstrated to date, with most demonstrated RISs in the lower frequency bands, either at microwave or mmW. The small unit cell sizes needed for operation in the sub-THz band makes fabrication and integration of reconfiguration components onto the unit cells very challenging compared to designs operating in the microwave regime. Table I summarizes the state-of-the-art RISs reported at the sub-THz band. According to Table I, the used reconfiguration technologies are based on either the electronic approach (CMOS transistors), functional materials (vanadium dioxide, VO_2) and liquid crystals), MEMS switches, or structural deformations using microfluidics. While the use of graphene is also possible, this approach has been mainly applied at the THz band [112], [113]. In terms of performance, 2D beamsteering with angles up to 60° has been reported [101]. On the other hand, reflective RISs typically have improved efficiency compared to transmissive ones. This is because the amplitude response of transmissive unit cells is typically below 0 dB, whereas reflective ground plane backed unit cells can achieve a near-unity (∼0 dB) amplitude response.

In terms of design approaches, the concept of metasurfaces has mainly been applied in the literature. While both transmissive and reflective RIS architectures have been adapted quite equally, a reflectarray-based design has also been demonstrated in this band. The majority of the reported reflective/transmissive beam reconfigurations have mainly adapted electrical (transistor) switching methods implemented using CMOS technology. While this technology offers a good alignment with existing IC-based processes (in which most front-end components are likely to be fabricated), the complexity of such solution increases with the required beamsteering resolution. In other words, more transistors may be required

TABLE II
COMPARISON OF DIFFERENT ANTENNA SOLUTIONS AND TECHNOLOGIES REPORTED AT UPPER MM-WAVE AND SUB-THz FREQUENCIES

Ref.	Antenna type	Operating freq. (GHz)	BW (GHz)	Peak gain (dBi)	Aperture size (λ^2)	Steering technology	Total steering angle (°)	Fabrication technology
[114]	Lens (single)	200–320	120	15	1.056×0.485	Fixed	Fixed	SiGe IC
[115]	Lens (single)	275	N/A	23.5	$\pi \times 10.5^2$	Electrical	15	3D printing
[116]	Lens array	340	N/A	15.7	6×6	Fixed	Fixed	3D printing
[117]	Patch array	314–323	9	8.6	3.6×3.6	Fixed	Fixed	0.13-µm BiCMOS
[118]	Slot array	118–133	15	43	134.4×134.4	Fixed	Fixed	Diffusion bonding
[119]	Phased array	318–370	52	4	0.977× 0.592	Electrical	128/53	0.13-µm BiCMOS
[56]	Phased array	370–410	40	15	3×3.5	Electrical	75	45-nm CMOS SOI
[59]	Phased array	300	N/A	2.3	32×21	OE	50	InP-based substrate
[120]	Phased array	90–100	10	21.1	29×6.5	Electrical	18/14	Standard PCB
[121]	Reflectarray	100	N/A	24.96	30×30	Fixed	Fixed	3D printing
[65]	Reflectarray	96–102	6	19.4	1.145×1.093	FM	55	–
[75]	Transmitarray	330	N/A	23.1	9.5×9.5	Fixed	Fixed	Standard PCB
[78]	Transmitarray	124–158	34	33.45	10.6×10.6	Fixed	Fixed	LTCC
[80]	Transmitarray	250	N/A	28.8	13.95×13.95	Fixed	Fixed	Standard PCB
[77]	Transmitarray	145	N/A	33	$\pi \times 10^2$	N/A	30	Standard PCB
[81]	LWA	230–330	100[a]	8.4	1.5×1.5	FS	88	InP-based substrate
[122]	LWA	325–400	75[a]	25.28	15.8×12.6	Electrical	22.7/60	MEMS micromachining
[86]	LWA	360–400	40[a]	4.5	3.8×1.3	FS	80	65-nm CMOS
[123]	DRA (single)	340	N/A	5.9	0.6×0.5	Fixed	Fixed	0.18-µm CMOS
[124]	DRA (single)	325	>163	8.6	0.87×0.87	Fixed	Fixed	65-nm CMOS
[125]	Bowtie + Lens	222–270	48	26.7	2.64×1.34	Fixed	Fixed	0.13-µm SiGe BiCMOS
[126]	LWA + Slot + Lens	250–500	250	28	$\pi \times 26^2$	FS	40	CMOS

LWA: Leaky-Wave Antenna; DRA: Dielectric Resonator Antenna; EM: Electro-Mechanical; FS: Frequency Sweep; OE: Opto-Electrical; FM: Functional Materials; LTCC: Low Temperature Co-fired Ceramic; PCB: Printed Circuit Board; CMOS: Complementary Metal-Oxide Semiconductor. [a]Instantaneous bandwidth.

to produce additional phase change steps across the overall steering range. Moreover, parasitics left over during the on-off switching of interconnecting sections in the unit elements using transistors may require compensation techniques.

Therefore, phase change materials and microfluidic techniques have been considered as potential alternatives. A well-designed microfluidic approach can offer a wide and continuous phase change, bounded only by the accuracy of the liquid actuation. On the other hand, the limited phase states and relatively high actuation voltages required in materials such as liquid crystals are also currently limiting their applicability in sub-THz reconfigurable antennas and RISs. Use of standard PCB technology becomes increasingly challenging at the sub-THz band due to the small unit cell sizes and the related difficulties in integrating reconfigurable electronics (transistors, diodes, etc.) on them. Therefore, most of the sub-THz PCB-based prototypes to date are customized reflectors designed to reflect waves to certain fixed angle(s) [75], [79], [109].

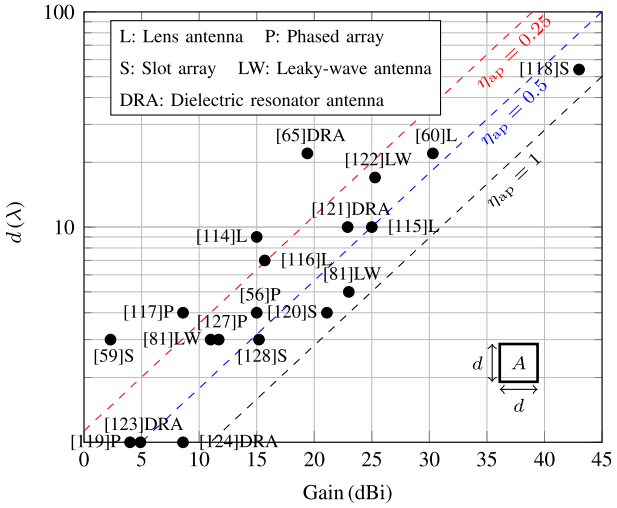

Fig. 12. Calculated antenna aperture dimension d as a function of measured gain to indicate the performance versus different η_{ap} limits.

IV. OBSERVATIONS ON SUB-THz ANTENNAS AND RISs

A. Outlooks for Sub-THz Antennas

Table II compares different antenna solutions reported in the sub-THz band in terms of operating frequency, gain, aperture size, utilized beam steering technology and achieved steering angle. The table shows that electrical beamsteering technology is the most common approach available at upper mmW and sub-THz bands due to its maturity. In general, a trade-off between the achieved gain and beam steering angles can be observed. For example, lenses and lens arrays feature the highest gains among the compared design, which is achieved at the expense of narrow beamsteering ranges. On the other hand, patch arrays produce relatively low gains while indicating reasonably wider beam steering angles.

Fig. 12 shows the gain of different types of antennas operating at the sub-THz band. It can be seen that most of the reported sub-THz antennas achieved gain values ranging from 10 to 25 dBi. It is worth noting that at 300 GHz, a target data rate of 100 Gbps can only be achieved with antennas (Rx and Tx) having gains of at least 23 dBi, assuming a link distance of 10 m using 4 bit per symbol modulation scheme and 30-GHz bandwidth [5]. The required gain increases dramatically to 55 dBi when the link distance extends to 1 km. From this calculation, it is obvious that the achieved gain of state-of-the-art sub-THz antennas are largely below the requirements. Moreover, the achieved gains are far from the

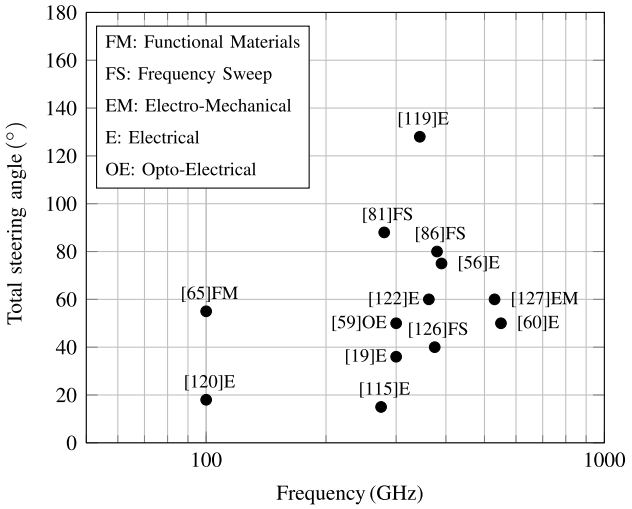

Fig. 13. Comparison of the scanning angles obtained with state-of-the-art beam-scanning sub-THz and THz antennas reported in the literature.

required values for a longer link distance, i.e, 1 km which is a common outdoor distance for communications. As expected, most lens antennas show a higher gain compared to array antennas and their variants (phased arrays, reflectarrays and transmitarrays).

As the achievable gain of an antenna depends on the aperture size and efficiency of the design, a theoretical limit of the aperture size of each antenna together with their corresponding expected gain is also provided. In Fig. 12, the achieved high gain clearly comes at the expense of a bigger aperture size. In addition to this, slot and leaky-wave antennas show some of the highest efficiencies among the reported antennas, thus providing a good hint of the realistic options of antennas in terms of high gains and compact designs.

Fig. 13 compares the total scanning angle obtained from the state-of-the-art sub-THz/THz antennas based on different technologies. It is well known that conventional mechanical steering technology can produce a full range of steering (360°). However, there is an absence of this technology at such high frequency band in the literature, foreseen due to the difficulty in mechanically changing and controlling very small angles. Moreover, assuming that a single antenna is used in this steering method, it is expected that the produced beam and direction changes rather linearly with the mechanical steering angles. In general, the state-of-the-art THz antennas provide a total steering angle of around 60° (corresponding to 30° on each side). Among the technologies, the electrical approach shows a wider steering angle compared to other technologies due to its maturity, which is widely studied and optimized.

The choice of proper sub-THz antenna design strategy depends on the gain, bandwidth and beam steering requirements. For example, for a fixed links with high gain and not required beamsteering, integrated lens antennas might be suitable solution. Meanwhile, for low-mobility applications, a switched-beam lens antenna could be optimal choice since it enables one or more simultaneous beams. Phased arrays have potential to show their advantage in the case of moderate gain and high mobility communications applications which can be an option at the cost of more complex RF front-end implementations [5]. On the other hand, transmit- and reflectarray antennas allow simplifying the complex RF front-end of the phased array since it separates the feeding source from the array. However, similar with the phased-array antennas, transmit- and reflectarrays might be more difficult to implement in practice when the antenna elements and their spacing become smaller than other IC components. Furthermore, hundreds or thousands of antenna elements may be required, which will necessitate a substantial number of RF switches. This, in turn, increases implementation complexity and leads to challenges in power consumption and temperature control. Due to the trade-offs between steering angles, which define the mobility and gain, suitable solutions for antenna system might include a combination of different basic high-gain antenna types.

B. Challenges With Sub-THz RISs

Despite the abundance of RIS demonstration in the microwave and mmW (e.g., [90], [91], [129]), the number of sub-THz hardware implementations remains limited. The main challenges are selection of suitable concepts/technologies for reconfiguration, integration of real-time control to the selected technology, fabrication complexity due to small physical dimensions etc, explained as follows.

1) Bandwidth: Coding metasurfaces have widely been proposed to digitally control steering angles [129]. When this approach is applied in a passive RIS hardware in practice, the phase difference between unit cells must be as consistent as possible. For example, a 1-bit coded reflecting metasurface requires two unit-cell conditions to produce phase responses of 0° and 180°. Such conditions can only be met across a narrow bandwidth due to the narrow natural bandwidth of the resonating metasurface elements [130], which starts to limit the functionality of the passive RIS. On the other hand, phase shifters can be connected to the same unit cell to produce the desired phase responses. Therefore, more phase values can be produced than from a shape-dependent passive RIS. However, the bandwidth of an active RIS still depends on the bandwidth of the phase shifters, which may be relatively narrow.

2) Reflection/Transmission Efficiency: In RISs, reducing the parasitic components in the metasurface-based approach is one of the main challenges to improve the reflection efficiency [131]. Fundamental reasons for this and a potential method to overcome it using perfect anomalous reflection (PAR) behavior are extensively discussed in [132]. The proposed approach relies on impedance matching and requires complex analyses and calculations. As a result, the PAR concept has been adapted to and integrated with digital control to systematically modify its reflection phase [133]. A potential drawback of this approach is the small unit cell sizes needed to produce a wider beamsteering angle. This poses a challenge in terms of fabrication for sub-THz RIS; thus, the increase of the unit cell sizes and trade-offs with efficiency and steering angle width in practice need further investigation. For the transmitting RIS, the scattering strongly degrades the transmitting efficiency of the RIS. Compared to a reflective RIS where the

reflection magnitude is always unity (0 dB) due to the existence of a metal ground plane, the magnitude of the transmission coefficient of the transmit RIS is significantly below that level (normally around 30% [107]) and requires a lot of optimization to suppress the undesired scattering components.

3) Limited Available Fabrication Technologies: In metasurface based RISs, the unit-cell periodicity is normally sub-wavelength, whereas the dimensions of the radiating sections of the unit cell are even much smaller. Assuming the lowest sub-THz band operating frequency of 100 GHz, the unit cell periodicity of $\lambda/10$ is then 0.3 mm, which makes using conventional PCB technologies very challenging due to the high accuracies needed. Complementary metal-oxide semiconductor (CMOS) technology, a common fabrication method for RF integrated circuits (RFICs), can be the most feasible method for sub-THz RISs. This process offers satisfactory fabrication accuracy and allows integrating other electronic components (transistor switches, amplifiers etc.) to enable their reconfiguration in terms of beam direction and frequency. However, CMOS is more costly, and it is difficult to fabricate a RIS with large aperture in a single tile.

4) Active vs Passive RIS Tradeoff: An active RIS can provide amplification and phase shift to signals arriving to the structure prior to reflection/refraction. On the other hand, passive RISs only features the latter, i.e., a RIS with phase shift only. A continuous phase change from 0° to 360° is ideally needed in both active and passive RISs. However, practical reconfigurability levels of RISs are restricted by the phase/amplitude resolution (N), where the number of bits used N produces 2^N individual phase values. This limitation governs the beamsteering resolution [66]. Moreover, the size of typical CMOS phase shifters and power amplifiers can be comparable to or larger than the unit cell size of a metasurface/array, which adds to the design complexity and further complicates their integration.

5) Reconfiguration Technologies: The limited availability of technologies for reconfiguration in the sub-THz band restricts the current implementations to conventional PCB, liquid crystal, microfluidic, phase change materials and CMOS transistor switching approaches. In reconfiguring these structures, concepts derived from metasurfaces, phased arrays and polarizers have mainly been implemented. Open questions remain related to the phase change resolution which, in turn, affects the reflection resolution. Other important considerations include the maximum operating bandwidth, width of reflection angles, and reflected efficiency and power achievable by each technology. No dedicated implementations of active sub-THz RISs, which integrates amplification components have been reported to date. Nevertheless, current experiments have proven that the previous design and fabrication concepts are generally suitable for providing a satisfactory initial idea about the performance expected from sub-THz RISs.

V. Future Trends in 6G Sub-THz Hardware

Based on the state-of-the-art hardware technologies reported in the literature, it is clear that a vast amount of possible solutions exist to implement the future of 6G wireless communications systems. This section lists some of the potential future trends to transform 6G from a vision into reality. Fig. 14 visualizes these trends and shows their interdependent nature.

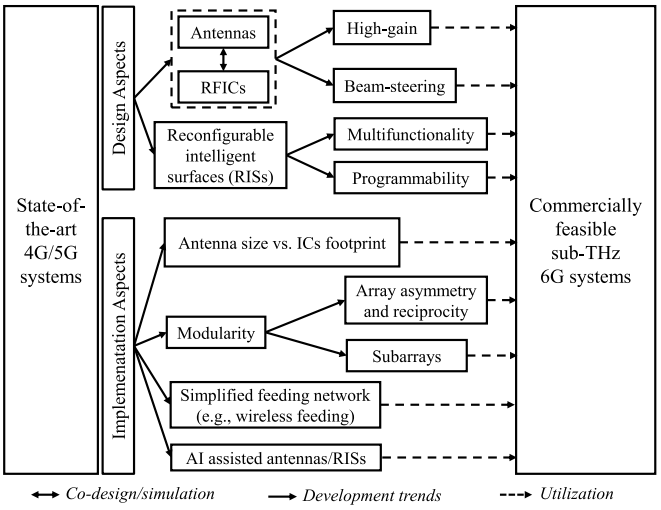

Fig. 14. Potential sub-THz hardware design trends for 6G.

A. Design Aspects

1) Co-Design and co-Simulation of Antennas and ICs: Antennas, analog, and digital electronics can no longer be designed and manufactured as independent components, as in the microwave regime. On the contrary, they need to be co-designed and co-integrated into a compact and multi-functional front-end ('system-on-chip') to conform to the compact physical space and size of the antenna-beamforming-IC component. During the development process, it is important that both antenna and circuit designers are aware of the key parameters and limitations that affect the performance.

2) Optimization of Energy Efficiency: The envisioned data rates of 6G mean that more bits will be transmitted per second. Together with the significantly increased complexity of the foreseen sub-THz 6G systems, this requires more signal processing and computing, ultimately increasing overall power consumption. To ensure sustainable 6G, careful consideration on energy efficiency is required. Energy efficiency not only applies to designing individual components and systems for efficient operation, but also to ensure that the energy is consumed only where it is truly needed. This again highlights the importance of antenna and RIS hardware reconfigurability. For instance, beam reconfigurability and amplification of radiation/reflection require additional energy due increased power consumption by phase shifters and amplifiers. Recently, it has been proposed that spectral and energy efficiency should be assessed in a volumetric way to account for the 3D nature of 6G [134], making the relevant metric bit/s/Hz/m^3/Joules.

3) Development of Multi-Functional and AI-Assisted RISs: Despite being foreseen to be an essential part of sub-THz communications, the development of RISs still leaves much to be desired, especially in terms of the "intelligence". Therefore, future RIS developments should include smarter AI-assisted controllers and algorithms. Furthermore, with such sophistication, an advanced RIS can be designed to switch between different working modes. Besides that, RIS can also be

integrated with sensing features, where the data can be fed to train the AI-based controllers. These sensors can either be a part of the RIS hardware or totally independent from it, even operating in another (lower) frequency band using established low-power methods in an integrated manner with the sub-THz hardware. Another area requiring hardware development is active RIS with power amplifiers. This aims to enhance the sub-THz link, as the RIS can amplify incident signals before reflecting them. Hybrid RISs (with partial power amplification) are also foreseent to have a big impact since they can balance between system performance and power consumption.

B. Implementation Aspects

1) Wireless Feeding Methods and IC-Based Fabrication for sub-THz Designs: Implementing ultra-compact electronics adhering to $\lambda/2$ or even sub-wavelength scaling toward higher frequencies is a major research topic. Firstly, methods to connect antenna elements to the RF front-ends (amplifiers, phase-shifters) using striplines at microwave regime should be revolutionized when working at the sub-THz band. Sub-THz antenna elements become smaller compared to the footprints of amplifiers or phase shifters. A solution is to use wireless feeding methods such as capacitive feeding [135]. Secondly, the fabrication cost of antennas and RISs can be higher due to the increased fabrication accuracy requirement, as standard low-cost PCB technologies (fabrication accuracies around 100 μm) become insufficient. Integration of the reconfiguration feature in sub-THz antennas/RISs is challenging using typical PCB or LTCC fabrication technologies due to the absence of commercial electronic components in this band. Therefore, the possibilities enabled by IC-based processes such as CMOS are envisioned to become the mainstream fabrication technology for reconfigurable sub-THz antennas/RISs.

2) Modularization of Subarrays for Scalable Implementations: The number of elements of antenna array and RIS are expected to be large to achieve highly directive beam(s). Together with feeding and control networks, the fabrication of such massive antennas/RISs becomes very challenging. Antenna/RIS subarray modularization (see, e.g., [136]) is envisioned as one critical technology to ensure that the systems are practically feasible and scalable. On the other hand, the use of subarrays can also affect the requirements of hybrid beamforming [137] and the achievable capacity [138]. Phased subarrays and hybrid beamforming together with extended array spacing provides an option to increase the angular resolution of mmW MIMO radar [139], which could prove relevant also at sub-THz frequencies. Extending the array spacing introduces grating lobes that can be suppressed through sum and difference subarray beams.

3) Reciprocity and Asymmetry in Antenna Arrays: Interesting aspects to consider for the array design are reciprocity [140] and aperiodic arrays [141]. Traditionally, arrays are designed to be reciprocal in transmission and reception. When moving towards sub-THz frequencies, it may be advantageous to design separate arrays for Tx and Rx, especially if the requirements and functionalities on either side of the link are highly different. Recently, the use of aperiodic antenna arrays has shown potential to improve the electrical and thermal performance (e.g. higher gain, less heat per element) over regular periodic arrays. Any possibilities to simplify the design, improve the performance and reduce the cost will be essential, as 6G sub-THz communications systems are to be produced in large numbers for the consumer market.

VI. Conclusion

This review article has presented an overview of the current state-of-the-art antennas and RIS hardware that have been experimentally demonstrated at the sub-THz band. It is known that due to the Shannon limits, increasingly congested spectrum and limited spectral availability motivates the need to operate the next generations of wireless communications with wider bandwidths at the mmW and sub-THz bands. Moreover, several white papers from major telecommunications industry players have indicated an interest in looking into the possibility to harness this advantage, especially using the sub-THz band. Approaches to the design of antennas and RISs at the sub-THz band can be rather different from the contemporary methods used at microwave frequencies. Scaling up antenna designs towards sub-THz and integrating unit elements into arrays may seem like a straightforward way, but this might not result in the desired performance without considerations of co-design, packaging, scalability, implementation methods and power consumption. Conventional interconnection and loss mitigation techniques may no longer be suitable for components at this band. Besides that, precision in fabrication is crucial in ensuring that small dimensions are realizable with smooth conductor surfaces to avoid the generation of unwanted or multi-mode radiations and reflections. It is foreseen that future key innovations in the sub-THz antenna hardware domain will arise from the demonstration of active and/or intelligent RISs and antennas with space-time coding and advanced beamforming features. Towards this end, the article has also suggested a number of research trends that can play a significant role in realizing the aims set for sub-THz wireless communications.

References

[1] H. Viswanathan and P. Mogensen. (2020). White paper: Communications in the 6G era. Nokia Bell Labs. [Online]. Available: https://www.bell-labs.com/institute/white-papers/communications-6g-era-white-paper/

[2] A. Pärssinen et al., "White paper on RF enabling 6G—Opportunities and challenges from technology to spectrum," 6G Res. Vis., Univ. Oulu, Oulu, Finland, White Paper 13, 2020. [Online]. Available: http://urn.fi/urn:isbn:9789526228419

[3] NTT Docomo. (2022). *White Paper: 5G Evolution and 6G*. [Online]. Available: https://www.docomo.ne.jp/english/corporate/technology/whitepaper6g/

[4] G. Wikström et al. (2022). 6G—Connecting a cyber-physical world. Ericsson. [Online]. Available: https://www.ericsson.com/4927de/assets/local/reports-papers/white-papers/6g–connecting-a-cyber-physical-world.pdf

[5] K. Rikkinen, P. Kyösti, M. E. Leinonen, M. Berg, and A. Pärssinen, "THz radio communication: Link budget analysis toward 6G," *IEEE Commun. Mag.*, vol. 58, no. 11, pp. 22–27, Nov. 2020.

[6] C. Wang et al., "0.34-THz wireless link based on high-order modulation for future wireless local area network applications," *IEEE Trans. THz Sci. Technol.*, vol. 4, no. 1, pp. 75–85, Jan. 2014.

[7] A. Hirata et al., "5.8-km 10-Gbps data transmission over a 120-GHz-band wireless link," in *Proc. IEEE Int. Conf. Wireless Inf. Technol. Syst.*, Honolulu, HI, USA, Aug./Sep. 2010, pp. 1–4.

[8] I. Kallfass, J. Antes, D. Lopez-Diaz, S. Wagner, A. Tessmann, and A. Leuther, "Broadband active integrated circuits for terahertz communication," in *Proc. 18th Eur. Wireless Conf.*, Poznań, Poland, Apr. 2012, pp. 1–5.

[9] I. Dan et al., "A 300-GHz wireless link employing a photonic transmitter and an active electronic receiver with a transmission bandwidth of 54 GHz," *IEEE Trans. THz Sci. Technol.*, vol. 10, no. 3, pp. 271–281, May 2020.

[10] P. Rodríguez-Vázquez, J. Grzyb, B. Heinemann, and U. R. Pfeiffer, "A 16-QAM 100-Gb/s 1-M wireless link with an EVM of 17% at 230 GHz in an SiGe technology," *IEEE Microw. Wireless Compon. Lett.*, vol. 29, no. 4, pp. 297–299, Apr. 2019.

[11] H. Hamada et al., "300-GHz-band 120-Gb/s wireless front-end based on InP-HEMT PAs and mixers," *IEEE J. Solid-State Circuits*, vol. 55, no. 9, pp. 2316–2335, Sep. 2020.

[12] I. Kallfass et al., "All active MMIC-based wireless communication at 220 GHz," *IEEE Trans. THz Sci. Technol.*, vol. 1, no. 2, pp. 477–487, Nov. 2011.

[13] H. J. Song, K. Ajito, Y. Muramoto, A. Wakatsuki, T. Nagatsuma, and N. Kukutsu, "24 Gbit/s data transmission in 300 GHz band for future terahertz communications," *Electron. Lett.*, vol. 48, no. 15, pp. 953–954, Jul. 2012.

[14] E. Lacombe et al., "10-Gb/s indoor THz communications using industrial Si photonics technology," *IEEE Microw. Wireless Compon. Lett.*, vol. 28, no. 4, pp. 362–364, Apr. 2018.

[15] P. Latzel et al., "THz transmission using QAM-16 and 32 Gbit/s on 25 m," in *Proc. 41st Int. Conf. Infr., Millim., THz Waves (IRMMW-THz)*, Copenhagen, Denmark, Sep. 2016, pp. 1–2.

[16] M. H. Eissa et al., "Wideband 240-GHz transmitter and receiver in BiCMOS technology with 25-Gbit/s data rate," *IEEE J. Solid-State Circuits*, vol. 53, no. 9, pp. 2532–2542, Sep. 2018.

[17] J. Grzyb, P. Rodríguez-Vázquez, S. Malz, M. Andree, and U. R. Pfeiffer, "A SiGe HBT 215–240 GHz DCA IQ TX/RX chipset with built-in test of USB/LSB RF asymmetry for 100+ Gb/s data rates," *IEEE Trans. Microw. Theory Techn.*, vol. 70, no. 3, pp. 1696–1714, Mar. 2022.

[18] S. Li, Z. Zhang, and G. M. Rebeiz, "An eight-element 136–147 GHz wafer-scale phased-array transmitter with 32 dBm peak EIRP and >16 Gbps 16 QAM and 64 QAM operation," *IEEE J. Solid-State Circuits*, vol. 57, no. 6, pp. 1635–1648, Jun. 2022.

[19] I. Abdo et al., "A bi-directional 300-GHz-band phased-array transceiver in 65-nm CMOS with outphasing transmitting mode and LO emission cancellation," *IEEE J. Solid-State Circuits*, vol. 57, no. 8, pp. 2292–2308, Aug. 2022.

[20] S. Ummethala et al., "Wireless transmission at 0.3 THz using direct THz-to-optical conversion at the receiver," in *Proc. Eur. Conf. Opt. Commun. (ECOC)*, Rome, Italy, Sep. 2018, pp. 1–3.

[21] F. Boes et al., "Ultra-broadband MMIC-based wireless link at 240 GHz enabled by 64GS/s DAC," in *Proc. 39th Int. Conf. Infr., Millim., THz Waves (IRMMW-THz)*, Tucson, AZ, USA, Sep. 2014, pp. 1–2.

[22] V. K. Chinni et al., "Single-channel 100 Gbit/s transmission using III–V UTC-PDs for future IEEE 802.15.3d wireless links in the 300 GHz band," *Electron. Lett.*, vol. 54, no. 10, pp. 638–640, May 2018.

[23] D. Fritsche, P. Stärke, C. Carta, and F. Ellinger, "A low-power SiGe BiCMOS 190-GHz transceiver chipset with demonstrated data rates up to 50 Gbit/s using on-chip antennas," *IEEE Trans. Microw. Theory Techn.*, vol. 65, no. 9, pp. 3312–3323, Sep. 2017.

[24] H. Hamada et al., "300-GHz. 100-Gb/s InP-HEMT wireless transceiver using a 300-GHz fundamental mixer," in *IEEE MTT-S Int. Microw. Symp. Dig.*, Philadelphia, PA, USA, Jun. 2018, pp. 1480–1483.

[25] S. Hara et al., "300-GHz CMOS transceiver for terahertz wireless communication," in *Proc. Asia–Pacific Microw. Conf. (APMC)*, Kyoto, Japan, Nov. 2018, pp. 429–431.

[26] S. Hara et al., "A 32 Gbit/s 16QAM CMOS receiver in 300 GHz band," in *IEEE MTT-S Int. Microw. Symp. Dig.*, Honolulu, HI, USA, Jun. 2017, pp. 1703–1706.

[27] S. Jia et al., "0.4 THz photonic-wireless link with 106 Gb/s single channel bitrate," *J. Lightw. Technol.*, vol. 36, no. 2, pp. 610–616, Jan. 15, 2018.

[28] I. Kallfass et al., "64 Gbit/s transmission over 850 m fixed wireless link at 240 GHz carrier frequency," *J. Infr., Millim., THz Waves*, vol. 36, no. 2, pp. 221–233, Feb. 2015.

[29] P. Rodriguez-Vazquez, J. Grzyb, B. Heinemann, and U. R. Pfeiffer, "A QPSK 110-Gb/s polarization-diversity MIMO wireless link with a 220–255 GHz tunable LO in a SiGe HBT technology," *IEEE Trans. Microw. Theory Techn.*, vol. 68, no. 9, pp. 3834–3851, Sep. 2020.

[30] T. Harter et al., "Generalized Kramers–Kronig receiver for coherent terahertz communications," *Nature Photon.*, vol. 14, no. 10, pp. 601–606, Oct. 2020.

[31] M. A. Uusitalo et al., "6G vision, value, use cases and technologies from European 6G flagship project Hexa-X," *IEEE Access*, vol. 9, pp. 160004–160020, 2021.

[32] Y. He, Y. Chen, L. Zhang, S.-W. Wong, and Z. N. Chen, "An overview of terahertz antennas," *China Commun.*, vol. 17, no. 7, pp. 124–165, Jul. 2020.

[33] C. A. Fernandes, E. B. Lima, and J. R. Costa, "Dielectric lens antennas," in *Handbook of Antenna Technologies*, Z. N. Chen, D. Liu, X. Qing, and T. Zwick, Eds. Singapore: Springer, 2016, pp. 1001–1065.

[34] G. M. Rebeiz, "Millimeter-wave and terahertz integrated circuit antennas," *Proc. IEEE*, vol. 80, no. 11, pp. 1748–1770, Nov. 1992.

[35] A. V. Boriskin, R. Sauleau, J. R. Costa, and C. Fernandes, "Integrated lens antennas," in *Aperture Antennas for Millimeter and Sub-Millimeter Wave Applications*, A. Boriskin and R. Sauleau, Eds. Cham, Switzerland: Springer, 2018, pp. 3–37.

[36] W. Hong et al., "Multibeam antenna technologies for 5G wireless communications," *IEEE Trans. Antennas Propag.*, vol. 65, no. 12, pp. 6231–6249, Dec. 2017.

[37] I. Lindell and K. Nikoskinen, *Antenniteoria*. Espoo, Finland: Otatieto, 1995.

[38] G. Markov, *Antennas*. Moscow, Russia: Progress Publishers, 1965.

[39] M. J. M. van der Vorst, P. J. I. de Maagt, and M. H. A. J. Herben, "Effect of internal reflections on the radiation properties and input admittance of integrated lens antennas," *IEEE Trans. Microw. Theory Techn.*, vol. 47, no. 9, pp. 1696–1704, Sep. 1999.

[40] N. T. Nguyen, R. Sauleau, M. Ettorre, and L. Le Coq, "Focal array fed dielectric lenses: An attractive solution for beam reconfiguration at millimeter waves," *IEEE Trans. Antennas Propag.*, vol. 59, no. 6, pp. 2152–2159, Jun. 2011.

[41] D. Headland, W. Withayachumnankul, M. Fujita, and T. Nagatsuma, "Integrated Luneburg and Maxwell fisheye lenses for the terahertz range," in *Proc. 44th Int. Conf. Infr., Millim., THz Waves (IRMMW-THz)*, Paris, France, Sep. 2019, pp. 1–2.

[42] H. Giddens, A. S. Andy, and Y. Hao, "Multimaterial 3-D printed compressed Luneburg lens for mm-wave beam steering," *IEEE Antennas Wireless Propag. Lett.*, vol. 20, no. 11, pp. 2166–2170, Nov. 2021.

[43] J.-M. Poyanco, F. Pizarro, and E. Rajo-Iglesias, "3D-printed dielectric GRIN planar wideband lens antenna for 5G applications," in *Proc. 15th Eur. Conf. Antennas Propag. (EuCAP)*, Düsseldorf, Germany, Mar. 2021, pp. 1–4.

[44] P. Pursula, A. Lamminen, R. Mannila, K. Tappura, and J. Saarilahti, "Silicon gradient refractive index lens for millimeter wave radiometers," in *Proc. 44th Int. Conf. Infr., Millim., THz Waves (IRMMW-THz)*, Paris, France, Sep. 2019, pp. 1–3.

[45] A. Lamminen, A. Tamminen, J. Saarilahti, V. Ermolov, and P. Pursula, "The effect of surface passivation for sub-THz silicon gradient refractive index lens," in *Proc. 51st Eur. Microw. Conf. (EuMC)*, London, U.K., Apr. 2022, pp. 873–876.

[46] B. Fuchs et al., "Comparative design and analysis of Luneburg and half Maxwell fish-eye lens antennas," *IEEE Trans. Antennas Propag.*, vol. 56, no. 9, pp. 3058–3062, Sep. 2008.

[47] O. Quevedo-Teruel et al., "Geodesic lens antennas for 5G and beyond," *IEEE Commun. Mag.*, vol. 60, no. 1, pp. 40–45, Jan. 2022.

[48] Q. Chen, S. A. R. Horsley, N. J. G. Fonseca, T. Tyc, and O. Quevedo-Teruel, "Double-layer geodesic and gradient-index lenses," *Nature Commun.*, vol. 13, no. 1, p. 2354, Apr. 2022.

[49] J. Zhu et al., "Additively manufactured millimeter-wave dual-band single-polarization shared aperture Fresnel zone plate metalens antenna," *IEEE Trans. Antennas Propag.*, vol. 69, no. 10, pp. 6261–6272, Oct. 2021.

[50] H. Jalili and O. Momeni, "A 436-to-467 GHz lens-integrated reconfigurable radiating source with continuous 2D steering and multi-beam operations in 65 nm CMOS," in *IEEE Int. Solid-State Circuits Conf. (ISSCC) Dig. Tech. Papers*, vol. 64, San Francisco, CA, USA, Feb. 2021, pp. 326–328.

[51] H. Jalili and O. Momeni, "A 0.46-THz 25-element scalable and wideband radiator array with optimized lens integration in 65-nm CMOS," *IEEE J. Solid-State Circuits*, vol. 55, no. 9, pp. 2387–2400, Sep. 2020.

[52] D. F. Filipovic, G. P. Gauthier, S. Raman, and G. M. Rebeiz, "Off-axis properties of silicon and quartz dielectric lens antennas," *IEEE Trans. Antennas Propag.*, vol. 45, no. 5, pp. 760–766, May 1997.

[53] R. J. Mailloux, *Phased Array Antenna Handbook*. Norwood, MA, USA: Artech House, 2017.

[54] M. Z. Chowdhury, M. Shahjalal, S. Ahmed, and Y. M. Jang, "6G wireless communication systems: Applications, requirements, technologies, challenges, and research directions," *IEEE Open J. Commun. Soc.*, vol. 1, pp. 957–975, 2020.

[55] X. Fu, F. Yang, C. Liu, X. Wu, and T. J. Cui, "Terahertz beam steering technologies: From phased arrays to field-programmable metasurfaces," *Adv. Opt. Mater.*, vol. 8, no. 3, Feb. 2020, Art. no. 1900628.

[56] Y. Yang, O. D. Gurbuz, and G. M. Rebeiz, "An eight-element 370–410-GHz phased-array transmitter in 45-nm CMOS SOI with peak EIRP of 8–8.5 dBm," *IEEE Trans. Microw. Theory Techn.*, vol. 64, no. 12, pp. 4241–4249, Dec. 2016.

[57] M. H. Mubarak, S. Hara, I. Watanabe, and A. Kasamatsu, "Beam steering in graphene-based sub-THz dipole phased array antenna," in *Proc. IEEE Int. Symp. Radio-Freq. Integr. Technol. (RFIT)*, Hiroshima, Japan, Sep. 2020, pp. 154–156.

[58] P. Lu et al., "Photonic assisted beam steering for millimeter-wave and THz antennas," in *Proc. IEEE Conf. Antenna Meas. Appl. (CAMA)*, Västerås, Sweden, Sep. 2018, pp. 1–4.

[59] M. Che, Y. Matsuo, H. Kanaya, H. Ito, T. Ishibashi, and K. Kato, "Optoelectronic THz-wave beam steering by arrayed photomixers with integrated antennas," *IEEE Photon. Technol. Lett.*, vol. 32, no. 16, pp. 979–982, Aug. 15, 2020.

[60] M. Alonso-delPino, S. Bosma, C. Jung-Kubiak, G. Chattopadhyay, and N. Llombart, "Wideband multimode leaky-wave feed for scanning lens-phased array at submillimeter wavelengths," *IEEE Trans. THz Sci. Technol.*, vol. 11, no. 2, pp. 205–217, Mar. 2021.

[61] P. Nayeri, F. Yang, and A. Z. Elsherbeni, *Reflectarray Antennas: Theory, Designs, and Applications*. Hoboken, NJ, USA: Wiley, 2018.

[62] J. Shaker, M. R. Chaharmir, and J. Ethier, *Reflectarray Antennas: Analysis, Design, Fabrication, and Measurements*. Norwood, MA, USA: Artech House, 2014.

[63] S. V. Hum and J. Perruisseau-Carrier, "Reconfigurable reflectarrays and array lenses for dynamic antenna beam control: A review," *IEEE Trans. Antennas Propag.*, vol. 62, no. 1, pp. 183–198, Jan. 2014.

[64] S. Bildik, S. Dieter, C. Fritzsch, W. Menzel, and R. Jakoby, "Reconfigurable folded reflectarray antenna based upon liquid crystal technology," *IEEE Trans. Antennas Propag.*, vol. 63, no. 1, pp. 122–132, Jan. 2015.

[65] G. Perez-Palomino et al., "Design and demonstration of an electronically scanned reflectarray antenna at 100 GHz using multiresonant cells based on liquid crystals," *IEEE Trans. Antennas Propag.*, vol. 63, no. 8, pp. 3722–3727, Aug. 2015.

[66] X. Meng, M. Nekovee, and D. Wu, "The design and analysis of electronically reconfigurable liquid crystal-based reflectarray metasurface for 6G beamforming, beamsteering, and beamsplitting," *IEEE Access*, vol. 9, pp. 155564–155575, 2021.

[67] Z. Hao, Z. Miao, and W. Hong, "Low profile terahertz antennas using the folded reflectarray," in *Proc. IEEE Int. Conf. Comput. Electromagn. (ICCEM)*, Singapore, Aug. 2020, pp. 25–26.

[68] S. Zhu, G. Wu, S. W. Pang, and C. Chan, "High–gain folded reflectarray antenna operating at 1 THz," in *Proc. 13th Global Symp. Millim.-Waves THz (GSMM)*, Nanjing, China, May 2021, pp. 1–3.

[69] A. Tamminen et al., "Reflectarray design for 120-GHz radar application: Measurement results," *IEEE Trans. Antennas Propag.*, vol. 61, no. 10, pp. 5036–5047, Oct. 2013.

[70] X. Liu, L. Schmitt, K. Kolpatzeck, M. Hoffmann, J. C. Balzer, and A. Czylwik, "Configuration of a MEMS-based terahertz reflectarray using a genetic algorithm," in *Proc. 46th Int. Conf. Infr., Millim. THz Waves (IRMMW-THz)*, Chengdu, China, Aug. 2021, pp. 1–2.

[71] E.-C. Choi and S. Nam, "Analysis and elimination of unwanted resonances for wideband reflectarray antenna design at sub-millimeter waves," *IEEE Access*, vol. 8, pp. 224750–224760, 2020.

[72] M. D. Wu et al., "Design and measurement of a 220 GHz wideband 3-D printed dielectric reflectarray," *IEEE Antennas Wireless Propag. Lett.*, vol. 17, no. 11, pp. 2094–2098, Nov. 2018.

[73] S. Sun, W. Li, and X. Shi, "A reconfigurable graphene reflectarray for generation of OAM in THz band," in *Proc. Int. Conf. Microw. Millim. Wave Technol. (ICMMT)*, Guangzhou, China, May 2019, pp. 1–3.

[74] A. H. Abdelrahman, F. Yang, A. Z. Elsherbeni, and P. Nayeri, "Analysis and design of transmitarray antennas," *Synth. Lect. Antennas*, vol. 6, no. 1, pp. 1–175, Jan. 2017.

[75] K. Medrar et al., "H-band substrate-integrated discrete-lens antenna for high data rate communication systems," *IEEE Trans. Antennas Propag.*, vol. 69, no. 7, pp. 3677–3688, Jul. 2021.

[76] O. Koutsos, F. F. Manzillo, A. Clemente, and R. Sauleau, "Analysis, rigorous design, and characterization of a three-layer anisotropic transmitarray at 300 GHz," *IEEE Trans. Antennas Propag.*, vol. 70, no. 7, pp. 5437–5446, Jul. 2022.

[77] F. F. Manzillo, A. Clemente, and J. L. González-Jiménez, "High-gain *D*-band transmitarrays in standard PCB technology for beyond-5G communications," *IEEE Trans. Antennas Propag.*, vol. 68, no. 1, pp. 587–592, Jan. 2020.

[78] Z. Miao et al., "140 GHz high-gain LTCC-integrated transmit-array antenna using a wideband SIW aperture-coupling phase delay structure," *IEEE Trans. Antennas Propag.*, vol. 66, no. 1, pp. 182–190, Jan. 2018.

[79] F. F. Manzillo, O. Koutsos, B. Fuchs, R. Sauleau, and A. Clemente, "Synthesis and characterization of a focused-beam transmitarray antenna at 300 GHz," in *Proc. 16th Eur. Conf. Antennas Propag. (EuCAP)*, Madrid, Spain, Mar. 2022, pp. 1–4.

[80] H. Yi, S.-W. Qu, and C. H. Chan, "Low-cost two-layer terahertz transmit array," *Electron. Lett.*, vol. 53, no. 12, pp. 789–791, Jun. 2017.

[81] P. Lu et al., "InP-based THz beam steering leaky-wave antenna," *IEEE Trans. THz Sci. Technol.*, vol. 11, no. 2, pp. 218–230, Mar. 2021.

[82] D. R. Jackson, C. Caloz, and T. Itoh, "Leaky-wave antennas," *Proc. IEEE*, vol. 100, no. 7, pp. 2194–2206, Jul. 2012.

[83] P. Baccarelli, P. Burghignoli, F. Frezza, A. Galli, and P. Lampariello, "Novel modal properties and relevant scanning behaviors of phased arrays of microstrip leaky-wave antennas," *IEEE Trans. Antennas Propag.*, vol. 51, no. 12, pp. 3228–3238, Dec. 2003.

[84] C. A. Balanis, *Modern Antenna Handbook*. Hoboken, NJ, USA: Wiley, 2011.

[85] M. Esquius-Morote, J. S. Gómez-Díaz, and J. Perruisseau-Carrier, "Sinusoidally modulated graphene leaky-wave antenna for electronic beamscanning at THz," *IEEE Trans. THz Sci. Technol.*, vol. 4, no. 1, pp. 116–122, Jan. 2014.

[86] H. Saeidi, S. Venkatesh, X. Lu, and K. Sengupta, "THz prism: One-shot simultaneous localization of multiple wireless nodes with leaky-wave THz antennas and transceivers in CMOS," *IEEE J. Solid-State Circuits*, vol. 56, no. 12, pp. 3840–3854, Dec. 2021.

[87] Y. Liu et al., "Reconfigurable intelligent surfaces: Principles and opportunities," *IEEE Commun. Surveys Tuts.*, vol. 23, no. 3, pp. 1546–1577, 3rd Quart., 2021.

[88] M. Di Renzo et al., "Smart radio environments empowered by reconfigurable intelligent surfaces: How it works, state of research, and the road ahead," *IEEE J. Sel. Areas Commun.*, vol. 38, no. 11, pp. 2450–2525, Nov. 2020.

[89] R. Liu, Q. Wu, M. Di Renzo, and Y. Yuan, "A path to smart radio environments: An industrial viewpoint on reconfigurable intelligent surfaces," *IEEE Wireless Commun.*, vol. 29, no. 1, pp. 202–208, Feb. 2022.

[90] W. Tang et al., "Wireless communications with reconfigurable intelligent surface: Path loss modeling and experimental measurement," *IEEE Trans. Wireless Commun.*, vol. 20, no. 1, pp. 421–439, Jan. 2021.

[91] L. Dai et al., "Reconfigurable intelligent surface-based wireless communications: Antenna design, prototyping, and experimental results," *IEEE Access*, vol. 8, pp. 45913–45923, 2020.

[92] M. A. ElMossallamy, H. Zhang, L. Song, K. G. Seddik, Z. Han, and G. Y. Li, "Reconfigurable intelligent surfaces for wireless communications: Principles, challenges, and opportunities," *IEEE Trans. Cogn. Commun. Netw.*, vol. 6, no. 3, pp. 990–1002, Sep. 2020.

[93] M. Di Renzo et al., "Reconfigurable intelligent surfaces vs. relaying: differences, similarities, and performance comparison," *IEEE Open J. Commun. Soc.*, vol. 1, pp. 798–807, 2020.

[94] M. Di Renzo, F. H. Danufane, X. Xi, J. D. Rosny, and S. Tretyakov, "Analytical modeling of the path-loss for reconfigurable intelligent surfaces—Anomalous mirror or scatterer?" in *Proc. IEEE 21st Int. Workshop Signal Process. Adv. Wireless Commun. (SPAWC)*, Atlanta, GA, USA, May 2020, pp. 1–5.

[95] M. Di Renzo, F. H. Danufane, and S. Tretyakov, "Communication models for reconfigurable intelligent surfaces: From surface electromagnetics to wireless networks optimization," *Proc. IEEE*, vol. 110, no. 9, pp. 1164–1209, Sep. 2022.

[96] W. Zhang et al., "Microfluid-based soft metasurface for tunable optical activity in THz wave," *Opt. Exp.*, vol. 29, no. 6, pp. 8786–8795, 2021.

[97] T. Q. H. Nguyen et al., "Simple design of a wideband and wide-angle reflective linear polarization converter based on crescent-shaped metamaterial for Ku-band applications," *Opt. Commun.*, vol. 486, May 2021, Art. no. 126773.

[98] S. Wang et al., "Arbitrary polarization conversion dichroism metasurfaces for all-in-one full Poincaré sphere polarizers," *Light, Sci. Appl.*, vol. 10, no. 1, pp. 1–9, Jan. 2021.

[99] J. Wang et al., "Metantenna: When metasurface meets antenna again," *IEEE Trans. Antennas Propag.*, vol. 68, no. 3, pp. 1332–1347, Mar. 2020.

[100] Y. Ra'di, D. L. Sounas, and A. Alù, "Metagratings: Beyond the limits of graded metasurfaces for wave front control," *Phys. Rev. Lett.*, vol. 119, no. 6, Aug. 2017, Art. no. 067404.

[101] N. M. Monroe, G. C. Doqiamis, R. Stingel, P. Myers, X. Chen, and R. Han, "Electronic THz pencil beam forming and 2D steering for high angular-resolution operation: A 98 × 98-unit 265 GHz CMOS reflectarray with in-unit digital beam shaping and squint correction," in *IEEE Int. Solid-State Circuits Conf. (ISSCC) Dig. Tech. Papers*, vol. 65, San Francisco, CA, USA, Feb. 2022, pp. 84–86.

[102] C. Liaskos, S. Nie, A. Tsioliaridou, A. Pitsillides, S. Ioannidis, and I. Akyildiz, "A new wireless communication paradigm through software-controlled metasurfaces," *IEEE Commun. Mag.*, vol. 56, no. 9, pp. 162–169, Sep. 2018.

[103] Q. Wu and R. Zhang, "Towards smart and reconfigurable environment: Intelligent reflecting surface aided wireless network," *IEEE Commun. Mag.*, vol. 58, no. 1, pp. 106–112, Jan. 2020.

[104] E. Björnson, Ö. Özdogan, and E. G. Larsson, "Intelligent reflecting surface versus decode-and-forward: How large surfaces are needed to beat relaying?" *IEEE Wireless Commun. Lett.*, vol. 9, no. 2, pp. 244–248, Feb. 2020.

[105] N. Rajatheva et al., "White paper on broadband connectivity in 6G," 6G Res. Vis., Univ. Oulu, Oulu, Finland, White Paper 10, 2020. [Online]. Available: http://urn.fi/urn:isbn:9789526226798

[106] G. Oliveri, D. H. Werner, and A. Massa, "Reconfigurable electromagnetics through metamaterials—A review," *Proc. IEEE*, vol. 103, no. 7, pp. 1034–1056, Jul. 2015.

[107] S. Venkatesh, X. Lu, H. Saeidi, and K. Sengupta, "A high-speed programmable and scalable terahertz holographic metasurface based on tiled CMOS chips," *Nature Electron.*, vol. 3, no. 12, pp. 785–793, Dec. 2020.

[108] Y. Liu et al., "Active tunable THz metamaterial array implemented in CMOS technology," *J. Phys. D, Appl. Phys.*, vol. 54, no. 8, Feb. 2021, Art. no. 085107.

[109] Y. Kato, K. Omori, and A. Sanada, "D-band perfect anomalous reflectors for 6G applications," *IEEE Access*, vol. 9, pp. 157512–157521, 2021.

[110] Q. Lin, H. Wong, L. Huitema, and A. Crunteanu, "Coding metasurfaces with reconfiguration capabilities based on optical activation of phase-change materials for terahertz beam manipulations," *Adv. Opt. Mater.*, vol. 10, no. 1, Jan. 2022, Art. no. 2101699.

[111] C. X. Liu et al., "Programmable manipulations of terahertz beams by transmissive digital coding metasurfaces based on liquid crystals," *Adv. Opt. Mater.*, vol. 9, no. 22, Nov. 2021, Art. no. 2100932.

[112] E. Carrasco, M. Tamagnone, and J. Perruisseau-Carrier, "Tunable graphene reflective cells for THz reflectarrays and generalized law of reflection," *Appl. Phys. Lett.*, vol. 102, no. 10, Mar. 2013, Art. no. 104103.

[113] M. Tamagnone et al., "Graphene reflectarray metasurface for terahertz beam steering and phase modulation," 2018, *arXiv:1806.02202*.

[114] B. Goettel, P. Pahl, C. Kutschker, S. Malz, U. R. Pfeiffer, and T. Zwick, "Active multiple feed on-chip antennas with efficient in-antenna power combining operating at 200–320 GHz," *IEEE Trans. Antennas Propag.*, vol. 65, no. 2, pp. 416–423, Feb. 2017.

[115] H. Yi, S. Qu, K. Ng, C. H. Chan, and X. Bai, "3-D printed millimeter-wave and terahertz lenses with fixed and frequency scanned beam," *IEEE Trans. Antennas Propag.*, vol. 64, no. 2, pp. 442–449, Feb. 2016.

[116] D. L. Guo, J. C. Mou, H. D. Qiao, W. Hu, and X. Lv, "A 2 × 2 3D printed micro-lens array for THz applications," in *Proc. 40th Int. Conf. Infr., Millim., THz Waves (IRMMW-THz)*, Hong Kong, Aug. 2015, pp. 1–2.

[117] W. Lin et al., "320 GHz on-chip circularly-polarized antenna array realized with 0.13 μm BiCMOS technology," in *Proc. IEEE Int. Symp. Antennas Propag. North Amer. Radio Sci. Meeting*, Toronto, ON, Canada, Jul. 2020, pp. 1467–1468.

[118] D. Kim, J. Hirokawa, M. Ando, J. Takeuchi, and A. Hirata, "64 × 64-element and 32 × 32-element slot array antennas using double-layer hollow-waveguide corporate-feed in the 120 GHz band," *IEEE Trans. Antennas Propag.*, vol. 62, no. 3, pp. 1507–1512, Mar. 2014.

[119] H. Jalili and O. Momeni, "A 0.34-THz wideband wide-angle 2-D steering phased array in 0.13-μm SiGe BiCMOS," *IEEE J. Solid-State Circuits*, vol. 54, no. 9, pp. 2449–2461, Sep. 2019.

[120] R. Klimovich, S. Jameson, and E. Socher, "W-band endfire 2-D phased-array transmitter based on ×9 CMOS active multiplier chips," *IEEE Trans. Antennas Propag.*, vol. 68, no. 12, pp. 7893–7904, Dec. 2020.

[121] P. Nayeri et al., "3D printed dielectric reflectarrays: Low-cost high-gain antennas at sub-millimeter waves," *IEEE Trans. Antennas Propag.*, vol. 62, no. 4, pp. 2000–2008, Apr. 2014.

[122] S. S. Yao, Y. J. Cheng, Y. F. Wu, and H. N. Yang, "THz 2-D frequency scanning planar integrated array antenna with improved efficiency," *IEEE Antennas Wireless Propag. Lett.*, vol. 20, no. 6, pp. 983–987, Jun. 2021.

[123] T. Chiu et al., "A 340-GHz high-gain flip-chip packaged dielectric resonator antenna for THz imaging applications," in *Proc. IEEE Int. Symp. Radio-Freq. Integr. Technol. (RFIT)*, Seoul, South Korea, Aug./Sep. 2017, pp. 123–125.

[124] S. Kong, K. M. Shum, C. Yang, L. Gao, and C. H. Chan, "Wide impedance-bandwidth and gain-bandwidth terahertz on-chip antenna with chip-integrated dielectric resonator," *IEEE Trans. Antennas Propag.*, vol. 69, no. 8, pp. 4269–4278, Aug. 2021.

[125] K. Schmalz et al., "Dual-band transmitter and receiver with bowtie-antenna in 0.13 μm SiGe BiCMOS for gas spectroscopy at 222–270 GHz," *IEEE Access*, vol. 9, pp. 124805–124816, 2021.

[126] S. van Berkel et al., "Wideband double leaky slot lens antennas in CMOS technology at submillimeter wavelengths," *IEEE Trans. THz Sci. Technol.*, vol. 10, no. 5, pp. 540–553, Sep. 2020.

[127] K. Guo, Y. Zhang, and P. Reynaert, "A 0.53-THz subharmonic injection-locked phased array with 63-μW radiated power in 40-nm CMOS," *IEEE J. Solid-State Circuits*, vol. 54, no. 2, pp. 380–391, Feb. 2019.

[128] M. Jiang, X. Lu, X. Xuan, R. Han, and M. Wang, "A THz slotted-waveguide array antenna based on MEMS technology," in *Proc. IEEE Asia–Pacific Conf. Antennas Propag. (APCAP)*, Auckland, New Zealand, Aug. 2018, pp. 238–240.

[129] T. J. Cui, M. Q. Qi, X. Wan, J. Zhao, and Q. Cheng, "Coding metamaterials, digital metamaterials and programmable metamaterials," *Light, Sci. Appl.*, vol. 3, no. 10, p. e218, Oct. 2014.

[130] X. G. Zhang et al., "Light-controllable digital coding metasurfaces," *Adv. Sci.*, vol. 5, no. 11, Nov. 2018, Art. no. 1801028.

[131] V. S. Asadchy, M. Albooyeh, S. N. Tcvetkova, A. Díaz-Rubio, Y. Ra'di, and S. A. Tretyakov, "Perfect control of reflection and refraction using spatially dispersive metasurfaces," *Phys. Rev. B, Condens. Matter*, vol. 94, no. 7, Aug. 2016, Art. no. 075142.

[132] A. Díaz-Rubio, V. S. Asadchy, A. Elsakka, and S. A. Tretyakov, "From the generalized reflection law to the realization of perfect anomalous reflectors," *Sci. Adv.*, vol. 3, no. 8, Aug. 2017, Art. no. e1602714.

[133] H. B. Jing, Q. Ma, G. D. Bai, and T. J. Cui, "Anomalously perfect reflections based on 3-bit coding metasurfaces," *Adv. Opt. Mater.*, vol. 7, no. 9, May 2019, Art. no. 1801742.

[134] W. Saad, M. Bennis, and M. Chen, "A vision of 6G wireless systems: Applications, trends, technologies, and open research problems," *IEEE Netw.*, vol. 34, no. 3, pp. 134–142, May/Jun. 2020.

[135] S. Li, Z. Zhang, B. Rupakula, and G. M. Rebeiz, "An eight-element 140 GHz wafer-scale phased-array transmitter with 32 dBm peak EIRP and > 16 Gbps 16QAM and 64QAM operation," in *IEEE MTT-S Int. Microw. Symp. Dig.*, Atlanta, GA, USA, Jun. 2021, pp. 795–798.

[136] M. J. W. Rodwell, A. S. H. Ahmed, M. Seo, U. Soylu, A. Alizadeh, and N. Hosseinzadeh, "IC and array technologies for 100–300 GHz wireless," in *Proc. IEEE Custom Integr. Circuits Conf. (CICC)*, Newport Beach, CA, USA, Apr. 2022, pp. 1–5.

[137] C. Han, L. Yan, and J. Yuan, "Hybrid beamforming for terahertz wireless communications: Challenges, architectures, and open problems," *IEEE Wireless Commun.*, vol. 28, no. 4, pp. 198–204, Aug. 2021.

[138] C. Lin and G. Y. Li, "Indoor terahertz communications: How many antenna arrays are needed?" *IEEE Trans. Wireless Commun.*, vol. 14, no. 6, pp. 3097–3107, Jun. 2015.

[139] K. Han and S. Hong, "High-resolution phased-subarray MIMO radar with grating lobe cancellation technique," *IEEE Trans. Microw. Theory Techn.*, vol. 70, no. 5, pp. 2775–2785, May 2022.
[140] W. Hong et al., "The role of millimeter-wave technologies in 5G/6G wireless communications," *IEEE J. Microw.*, vol. 1, no. 1, pp. 101–122, Jan. 2021.
[141] Y. Aslan, A. Roederer, and A. Yarovoy, "System advantages of using large-scale aperiodic array topologies in future mm-wave 5G/6G base stations: An interdisciplinary look," *IEEE Syst. J.*, vol. 16, no. 1, pp. 1239–1248, Mar. 2022.

Kimmo Rasilainen (Member, IEEE) was born in Helsinki, Finland, in 1987. He received the B.Sc. (Tech.), M.Sc. (Tech.) (Hons.), and D.Sc. (Tech.) degrees in electrical engineering from the School of Electrical Engineering, Aalto University, Espoo, Finland, in 2012, 2013, and 2017, respectively.

From 2009 to 2017, he was with the Department of Electronics and Nanoengineering, School of Electrical Engineering, Aalto University, first as a Research Assistant and later as a Research Scientist, working on handset antennas and wireless sensors. From 2017 to 2020, he was a Post-Doctoral Researcher with the Department of Microtechnology and Nanoscience, Chalmers University of Technology, Gothenburg, Sweden, working on the integration of mm-wave communications assemblies and thermal simulations. Since 2020, he has been a Post-Doctoral Researcher with the Centre for Wireless Communications, University of Oulu, Finland. He has authored or coauthored more than 40 international journal articles and conference papers. His current research interests include mm-wave and THz antennas, microwave engineering, and thermal analysis.

Tung Duy Phan (Member, IEEE) received the M.Sc. degree in radio engineering from Tula State University, Tula, Russia, in 2015, and the D.Sc. degree in electrical engineering from the Seoul National University of Science and Technology, Seoul, South Korea, in 2021.

From 2015 to 2018, he was a Lecturer with the School of Engineering and Technology, Vinh University, Vietnam. Since September 2021, he has been a Post-Doctoral Research Fellow with the Centre for Wireless Communications, University of Oulu, Oulu, Finland. He is the author/coauthor of over 25 peer-reviewed journals and conference publications. His research interests include sub-THz reconfigurable antennas and surfaces, optically transparent antennas, and electromagnetic shielding. He received the Best Paper Award from the IEIE Autumn Annual Conference in 2019, the Vietnamese Young Scientists in Korea Awards, the Best Ph.D. Thesis Award in 2021, and the IEEE Antennas and Propagation Society Fellowship (APSF) in 2022.

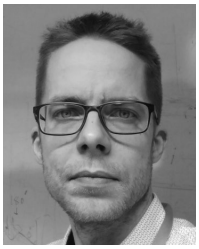

Markus Berg received the M.Sc. (Tech.) and D.Sc. (Tech.) degrees in electrical engineering from the University of Oulu, Oulu, Finland, in 2005 and 2011, respectively.

From 2005 to 2017, he was a Research Scientist and a Project Manager with the Centre for Wireless Communications, University of Oulu. In 2015, he was a Design Engineer with Elektrobit, Oulu, and Bittium Corporation, Oulu. Since 2017, he has been a Senior Research Fellow and an Adjunct Professor with the Faculty of Information Technology and Electrical Engineering, University of Oulu. In 2018, he founded ExcellAnt Ltd., where he is currently a Chief Technology Officer. He has authored or coauthored more than 90 international journal articles and conference papers. He holds one patent. His current research interests include antennas and propagation for wireless communication and radars, millimeter and sub-THz integrated antennas, and GNSS reflectometry.

Aarno Pärssinen (Senior Member, IEEE) received the M.Sc., Licentiate in Technology, and Doctor of Science degrees in electrical engineering from the Helsinki University of Technology, Helsinki, Finland, in 1995, 1997, and 2000, respectively.

From 1994 to 2000, he was with the Electronic Circuit Design Laboratory, Helsinki University of Technology, working on direct conversion RXs and subsampling mixers for wireless communications. In 1996, he was a Research Visitor with the University of California at Santa Barbara, Santa Barbara, CA, USA. From 2000 to 2011, he was with the Nokia Research Center, Helsinki. From 2011 to 2013, he was with Renesas Mobile Corporation, Helsinki, as a Distinguished Researcher and the RF Research Manager. From October 2013 to September 2014, he was an Associate Technical Director with Broadcom, Helsinki. Since September 2014, he has been with the Centre for Wireless Communications, University of Oulu, Oulu, Finland, where he is currently a Professor. He is leading the devices and circuits research area in the 6G flagship program financed by the Academy of Finland. He is one of the original contributors to Bluetooth low energy extension, now called BT LE. He has authored or coauthored one book, two book chapters, and more than 200 international journal articles and conference papers. He holds several patents. His research interests include wireless systems and transceiver architectures for wireless communications with special emphasis on radio frequency (RF) and analog integrated circuits and system design.

Dr. Pärssinen served as a member of the Technical Program Committee for the International Solid-State Circuits Conference from 2007 to 2017, where he was the Chair of the European Regional Committee from 2012 to 2013 and the Wireless Sub-Committee from 2014 to 2017. From 2009 to 2011, he served as a member for the Nokia CEO Technology Council. He has served as a Solid-State Circuits Society Representative for the IEEE 5G Initiative from 2015 to 2019.

Ping Jack Soh (Senior Member, IEEE) received the Ph.D. degree in electrical engineering from KU Leuven, Belgium.

He started his career as a Test Engineer (2002–2004) and a Research and Development Engineer (2005–2006) in two telecommunication/electronics companies. He was a Lecturer with Universiti Malaysia Perlis (UniMAP) (2006–2009) before moving to KU Leuven as a Research Assistant (2009–2013) and a Post-Doctoral Research Fellow (2013–2014). He has been a Research Affiliate since 2014. He rejoined UniMAP as a Senior Lecturer (2014–2017) and an Associate Professor (2017–2021), before his current role. He is currently an Associate Professor with the University of Oulu, Finland, and the Coordinator of the "Devices and Circuit Technology" strategic research area within the Finnish National 6G Flagship Research Program. To date, he has led and completed five internationally- and nationally-funded research projects as the Principal Investigator, besides currently leading ongoing projects funded by the Academy of Finland, the U.S. Office of Naval Research Global, and Horizon Europe. He has published more than 300 articles (more than 140 in journals), four book chapters, and five invention disclosures. His research interests include antenna design and its applications in wearables/wireless body area communication (WBAN), metasurfaces and reflectors, next-generation communications, compact satellites, EM safety and absorption, and wireless techniques for healthcare.

Dr. Soh is a member of the IET and URSI. He was a recipient of the URSI Young Scientist Award in 2015, the IEEE Microwave Theory and Techniques Society (MTT-S) Graduate Fellowship for Medical Applications in 2013, and the IEEE Antennas and Propagation Society (AP-S) Doctoral Research Award in 2012. He was also the Second Place Winner of the IEEE Presidents' Change the World Competition in 2013. He is also serving as the TPC Co-Chair for the IEEE MTT-S International Microwave Biomedical Conference (IMBioC) 2023. He also volunteers in the IEEE MTT-S Education Committee. He serves as an Associate Editor for the IEEE ANTENNAS AND WIRELESS PROPAGATION LETTERS and the *International Journal of Numerical Modelling: Electronic Networks, Devices and Fields* (Wiley). He is a Chartered Engineer registered with the U.K. Engineering Council.